International Journal of Fatigue 189 (2024) 108565

Contents lists available at ScienceDirect

International Journal of Fatigue

journal homepage: www.elsevier.com/locate/ijfatigue

Fatigue assessment of structural components through the Effective Critical Plane factor

A. Chiocca *, F. Frendo

Department of Civil and Industrial Engineering, University of Pisa, Pisa, Italy

ARTICLE INFO

Keywords:
Critical plane method
Fatigue assessment
Computational cost
Control volume
Notched component
Volumetric average

ABSTRACT

The integrity assessment of structural components under complex loading conditions relies on the evaluation of the fatigue damage typically arising from stress concentrations, such as geometric irregularities, notches, weld beads, grooves etc.. Various methodologies, including the Notch Stress Approach (NSA), the Theory of Critical Distances (TCD), the Strain Energy Density (SED), and the Critical Plane (CP) concept, have been pivotal in assessing fatigue strength for notched and welded components. Recent works combine some of the above mentioned methodologies, while other works propose to vary the embedded parameters accounting for the loading type or the fatigue lives, trying to improve the accuracy of the fatigue assessment process. This paper introduces a novel approach, the Effective Critical Plane (ECP), which is founded on the critical plane concept. The CP factor is, however, calculated starting from an averaged, over a small volume, stress–strain field. The size of the averaging volume is assumed to be a material parameter and is determined by a best fitting procedure over different experimental data sets. The novel approach is illustrated by means of the *Fatemi-Socie* and the *Smith-Watson-Topper* CP damage factors. Its potential application to other CP formulations is straightforward, as well. Literature experimental data for low carbon steel specimens possessing different notches and loading conditions are used to validate the method's capability in accurately determining the fatigue life and to set the radius of the averaging volume for the given material and CP parameter. A spherical volume or circular area are used in case of fully 3D or 2D numerical models, respectively. Results are compared to those of some of already existing methods, namely SED, TCD and the Modified Wöhler Curve Method.

1. Introduction

Fatigue assessment of structural parts has continuously evolved, since the first fatigue-associated disasters, to safeguard the integrity of components subjected to complex loading conditions. The critical evaluation of the fatigue damage originating at stress concentrators, induced by geometric irregularities, constitutes the heart of this assessment. Notches, weld beads, grooves, material defects and similar features act as stress raisers, exerting significant influence on the fatigue life of machine elements [1].

Over time, several methodologies have emerged to account for the fatigue assessment of notched components, including some well established in the industrial scenario and related to technical standards [2–4] and others more typically used in theoretical and applied research contexts. Among these, methods such as the Notch Stress Approach (NSA) [5,6], the Theory of Critical Distances (TCD) [7,8], the Strain Energy Density (SED) [9–13] and Critical Plane (CP) [14–18] have held significant momentum during the last decades. The NSA, based on the fundamental works by Olivier et al. [19] and Radaj [20], followed the original idea of Neuber's micro-support theory to evaluate an effective stress (stress average over a small process volume), obtained as the local stress evaluated at a fictitious notch rounding radius (typically 1 mm or 0.05 mm depending on the metal thickness) [6,21,22]. The TCD, conceptualized by Taylor [23] and refined by Susmel and Taylor [24], assesses critical conditions according to stress parameters evaluated at specific distances or averaged over critical dimensions. This methodology couples stress parameters in notched or cracked components with fatigue failure of smooth parts. Conversely, the SED approach, rooted in the pioneering work of Sih [25] and subsequently refined by Lazzarin and Zambardi [26] and Lazzarin and Berto [9], hinges on a critical mean value of the strain energy density within control volumes or areas. All the above methods determine an averaged effective parameter over a given distance or process volume to be used for the fatigue assessment.

Critical Plane (CP) methodologies, originated in the second half of the 20th century, integrate a conceptual understanding of the fracture mechanisms inherent in the material to establish an equivalent

* Corresponding author.
E-mail addresses: andrea.chiocca@unipi.it (A. Chiocca), francesco.frendo@unipi.it (F. Frendo).

https://doi.org/10.1016/j.ijfatigue.2024.108565
Received 21 May 2024; Received in revised form 13 August 2024; Accepted 15 August 2024
Available online 22 August 2024

damage coefficient. They are based on the experimental observation that in polycrystalline materials cracks originate at given preferred orientations, where a critical combination of shear and normal stress–strain components exists, depending on the class of material and on the loading conditions; along with the critical damage parameter, these methods identify a critical orientation, along which the fatigue crack initially propagates.

The finite elements analysis (FEA) is ususally employed to deal with complex geometries or load histories, allowing to take into consideration factors such as load phase shifting, multiaxiality and mean stresses [27–35]. To this regard the CP methods can inherently account for load phase and mean stress variations. However, their implementation is way more challenging with respect to other methods such as NSA, TCD and SED. Until recently, challenges persisted in reconciling computational efficiency with accuracy, particularly for CP methods. Efforts to ease computational burdens have encompassed closed-form solutions and algorithms that aim to simplify the identification of critical planes and factors. Susmel et al. [36] formulation allows finding the orientations of the critical plane for generic load histories using the maximum variance method. Marques et al. [37] introduced an algorithm for spectral methods that facilitates a more efficient tracking of critical plane factors and stress variance directions. Alternative methods focus on computational speed by computing critical plane factors only for specific planes, avoiding discretizing the entire space with a fixed angular increment. Techniques such as the algorithm of Wentingmann et al. [38] segment a coarse Weber half sphere with quad elements to speed up the detection of critical planes, while Sunde et al. [39] developed an adaptive scheme that densifies a triangular mesh around areas with significant damage observations to improve the computational efficiency.

The above mentioned approaches have demonstrated considerable success in the evaluation of the fatigue strength of structural components under a spectrum of loading conditions, providing valuable insights into structural integrity [7,10,40–49]. However, the need for more precise fatigue assessments has directed attention to the fundamental parameters governing TCD, SED and CP methodologies namely critical distances, control radii and material parameters. In this context, some examples are provided by the reverse search procedures proposed by Santus et al. [50,51], which attempted to robustly determine the TCD critical length through severely notched specimens as an alternative option to the use of the plain specimen fatigue limit. Pedranz et al. [52] introduced a multiaxial fatigue criterion based on SED that handles both the mean stress effect and phase effect. Other authors have computed CP factors under variable material parameters; to this regard, Karolczuk et al. [53] enhance the *Fatemi-Socie* damage model by introducing a material parameter dependent on the fatigue life and evaluate it using the *Chaboche* hardening plasticity model for stress calculation.

More recently, some authors have tried to combine the CP method with other theories. Among these, Santus et al. [54], after numerically replicating the residual stresses distribution of notched and shot peened specimens, calculated critical distances using the Line Method (LM) and the SWT critical plane criterion. Queiroz et al. [55] and Araujo et al. [56] introduced a novel coupled critical plane-$\sqrt{\text{area}}$ methodology tailored to estimate the fatigue life within the medium and high number of cycles regime. The study proposes adaptations of the FS, SWT, and the Modified Wöhler Curve Method (MWCM) multiaxial criteria, integrating the $\sqrt{\text{area}}$ parameter developed by Murakami and Endo [57] to better account for the presence of defects in fatigue life estimation. Liao et al. [58] investigated different fatigue analysis techniques for notched components under multiaxial loading conditions, exploring combinations of the FS CP approach with the TCD Point Method (PM) and LM. Liu et al. [59] presented a novel probabilistic model for notched specimens under multiaxial loading, achieved by integrating the Weakest Link Theory (WLT) and the CP approach. They introduced the concept of effective stress derived from WLT and Weibull distribution and defined a critical damage region on the critical plane to account for size effect. In a recent work, Carpinteri et al. [60] introduces an extension of the Carpinteri-Spagnoli (CS) critical plane criterion by combining it with the SED concept. The fatigue strength evaluation is conducted at a designated point in the material located at a radial distance r from the notch tip. The distance r, determined along the bisector line of the notch (on the basis of TCD), is associated with the average radius of the SED control volume, which is calculated by averaging the radii relative to Mode I and Mode III. Luo et al. [61] proposed a method based on a local stress response to identify the fatigue critical point on the notch edge. This critical point, determined by maximum local peak stress, defines the material point where the critical plane, defined based on the maximum shear stress amplitude, passes through. Along the CP direction, the TCD is finally applied to calculate an equivalent maximum normal stress and shear stress amplitude, in order to define the damage parameter.

It has to be noted that all these methods make use and combine, in different ways, different theories. In addition, some of the earlier approaches, such as SED or TCD, use a scalar parameter, or a single stress component, losing a great amount of information, which may, actually, significantly affect the fatigue life. This aspect has been evidenced in some recent researches, e.g. the difficulty of the SED method in accounting for mean stress sensitivity and multiaxial non proportional loading conditions has been discussed by Pedranz et al. [52], while Susmel and Taylor [62] apply the TCD in combination with MWCM to account for non-zero mean stress and non-proportional loading conditions.

As opposite to that, a novel approach, the Effective Critical Plane (ECP) factor is proposed in this work, which uses the CP concept and stress–strain averaging around a notch. It is worth noting that the CP concept, which has been supported in many studies by the phenomenological observation on the early fatigue cracks, preserves the inherent tensorial characteristics of the stress–strain field, which allows to fully take account of generally complex loading conditions that can actually influence the fatigue failure process. Similarly, it does not rely on using any predetermined direction, such as notch bisector line of TCD, which, for some complex 3D geometries, such as lattice structures or porous materials, may even result difficult to be defined.

The work can be considered as a natural follow up of the authors' previous work, since it exploits the developments in the computational efficiency of CP damage parameters recently presented in [63–67], and make use of the volumetric averaging of the stress field around a notch. Indeed, it is a common assumption that fatigue crack originates over a process volume and that the maximum local stress evaluated at a notch by a linear elastic analysis has limited value. This holds also for CP analysis. Such assumption is supported by several considerations, such as the differences in the local geometry (e.g. notch radius) that can be present between the real case and the numerical model, or any possible local yielding in the material, which is not considered in a linear analysis, or cases where singularities are present in the elastic solution. It is also enforced by the evidence that at the meso-scale the material cannot be considered as an elastic continuum (there are grains and grain boundaries with given distribution and orientation) and, as a consequence, the elastic solution obtained at any given point by a numerical model does not represent the actual stress–strain in the material.

The ECP method consists in calculating the CP parameter at a given (critical) point, starting from the averaged stress–strain field, obtained over a very small volume, centred at that location. The critical location is defined as the material points with the largest value of the selected critical plane factor. In case of fully 3D geometry a small sphere, while for 2D geometries a circular area will be utilized for the averaging process. In both cases, the radius (i.e. called control radius) is assumed to be a material parameter, which has to be determined by a single variable fitting procedure.

The proposed methodology is based on the premise that accurate assessments can be obtained by considering linear elastic stress distributions near stress concentration zones and this assumption offers considerable simplification. It makes it possible to deal effectively with three-dimensional stress conditions induced by complex external force systems by using the superposition principle. With the aim of discussing the new approach in comparison to some other methods already available in the literature, in the first part of the paper an explanatory overview is provided, involving two of the most commonly employed CP parameters, i.e. the *Fatemi-Socie* and the *Smith-Watson-Topper* CP factors (i.e. the method can be easily applied to any other CP formulation, as well). Following this, fatigue test results taken from the literature for low carbon steel specimens having various notches and subjected to several loading conditions, are used to derive the optimal value of the control radius for the selected material and validate the method's capability in performing fatigue life evaluation. The outcomes of the research are finally used to draw some considerations, in comparison with some other local methods for fatigue assessment.

2. Method - effective critical plane factor

The method is introduced with reference to the *Fatemi-Socie* (FS) [14] and *Smith-Watson-Topper* (SWT) [68] CP factors; however, it can be easily adapted to other CP formulations.

The FS parameter is given in Eq. (1):

$$\mathrm{FS} = \frac{\Delta\gamma_{max}}{2}\left(1 + k\frac{\sigma_n}{\sigma_y}\right) \tag{1}$$

where k represents the material parameter usually determined through a fitting process between uniaxial and torsional data, $\frac{\Delta\gamma_{max}}{2}$ represents the maximum shear strain amplitude, σ_n is the maximum normal stress experienced during the load cycle on the plane where the maximum shear strain amplitude is found and σ_y is the material's yield strength. Such formulation is typically employed to investigate the shear-cracking phenomenon which is observed in some materials, being founded on the maximum shear strain range.

The SWT CP factor, including Socie's modification, is given in Eq. (2):

$$\mathrm{SWT} = \frac{\Delta\varepsilon_{max}}{2}\sigma_n \tag{2}$$

where $\frac{\Delta\varepsilon_{max}}{2}$ represents the amplitude of the maximum normal strain, while σ_n represents the maximum value of the normal stress acting on the maximum normal strain plane during the load cycle. The SWT CP factor is commonly utilized for materials prone to tensile cracking, in contrast to the FS model.

The ECP method uses a small process volume over which the stress field is averaged. The size of this process volume is a material parameter and has to be determined by a best fit procedure over different fatigue experimental data. For this reason, at least, two different notched specimen geometries are required (these are idealized by the two specimens represented in Fig. 1a).

The first step for the novel approach is the identification of the node j in the FE model, with the maximum value of the selected CP factor:

$$j = \arg\max_i \mathrm{CP}_i \tag{3}$$

where i represent the index of the generic node. Then, the spatial averaging over a given process volume of the stress–strain field obtained with a linear elastic analysis is carried out. Having defined $\mathbf{x}_i$ and $\mathbf{x}_j$ as the coordinates of node i and those of node j, the condition for a node i to be within the averaging volume (i.e. a sphere having radius r_c and centred at node j) is given by:

$$\|\mathbf{x}_i - \mathbf{x}_j\| \le r_c \tag{4}$$

where r_c is a first choice of the radius of the process volume.

The volumetric averaged stress and strain tensors are simply given by:

$$\bar{\sigma} = \frac{\sum_i \sigma_i \,\mathrm{IND}(\|\mathbf{x}_i - \mathbf{x}_j\| \le r_c)}{N} \tag{5}$$

and

$$\bar{\varepsilon} = \frac{\sum_i \varepsilon_i \,\mathrm{IND}(\|\mathbf{x}_i - \mathbf{x}_j\| \le r_c)}{N} \tag{6}$$

where, IND(•) is a function that returns 1 if the condition inside parentheses is true and 0 otherwise and N is the number of nodes within the averaging volume.

Once the averaged stress and strain tensors have been obtained, the effective critical plane parameter (ECP), $\widetilde{\mathrm{FS}}$ or $\widetilde{\mathrm{SWT}}$, can be calculated, e.g. by employing one of the closed form solution already presented by the authors. The procedure outlined in [65,69] can be used in case of linear elasticity and proportional loading, while the formulations described in [63,66] can be applied in case of more generic non proportional loading or material plasticity conditions. In the present work, the algorithm developed in [63] was used for both FS and SWT, as non-proportional loading conditions are present among the experimental data taken from the literature.

The overall procedure is implemented through finite element analysis, as shown in Fig. 1a. Linear-elastic simulations under unitary loads can be carried out for the subsequent steps. As usually done, in case of FE analyses, a preliminary convergence analysis is necessary to assure that, at least inside the control volume, the FE results do not depend on the mesh size. The convergence is not guaranteed only in case of notches having null radius, but this do not represent a real case. Following the FE analysis, the *Fatemi-Socie* and *Smith-Watson-Topper* ECP factors can be easily obtained for any given load value F, by the following Eqs. (7)–(8), which simply derive from Eqs. (1)–(2):

$$\widetilde{\mathrm{FS}} = \frac{\widetilde{\Delta\gamma}_{max}}{2}F + \frac{k}{2\sigma_y}\widetilde{\Delta\gamma}_{max}\widetilde{\sigma}_n F^2 \tag{7}$$

$$\widetilde{\mathrm{SWT}} = \frac{\widetilde{\Delta\varepsilon}_{max}}{2}\widetilde{\sigma}_n F^2 \tag{8}$$

The tilde in previous equation signifies that $\widetilde{\Delta\gamma}_{max}$, $\widetilde{\Delta\varepsilon}_{max}$ and $\widetilde{\sigma}_{n,}$ are obtained starting form the averaged values of the stress and strain tensors ($\bar{\sigma}$ and $\bar{\varepsilon}$) over the given (first choice) control radius r_c, under a unitary load. It is worth noting that, the load labelled F denotes any conditions of external loads existing on the component, which can be provided by either forces or moments (e.g. in the case of multiaxial loading condition F can refer to a specific value of either the tensile or the torsion loading).

Since the previous steps have been referred to a first choice of the control radius r_c, it is now possible to evaluate the averaged stress and strain tensor for different values of r_c (see Fig. 1b) and, as a consequence, to obtain the $\widetilde{\mathrm{FS}}$ and $\widetilde{\mathrm{SWT}}$ ECP factors vs r_c, for the two specimen geometries, as shown in Fig. 1c.

Now, matching the $\widetilde{\mathrm{FS}}$ and $\widetilde{\mathrm{SWT}}$ with the experimental number of cycles to failure corresponding to different load values (see Fig. 1d), a reference endurance curve can be obtained for a given choice of the control radius r_c, as illustrated in Fig. 1e.

A further step is then necessary in order to calibrate the method, by obtaining the optimal r_c. This is accomplished by a fatigue scatter (i.e $\mathrm{T_{ECP}}$) minimization process. At least two different notched geometries have to be used (as represented in Fig. 1). The control radius r_c that provides the minimum scatter on the calibration dataset is selected as the optimal control radius for the given material. The resulting fatigue endurance curve has to be considered as the reference curve for the fatigue design with that material and CP factor.

For the sake of clarity, the method was explained considering two specimen geometries and a single loading mode. It should be considered that, in order to obtain a robust master curve for a given material, experimental results obtained with different geometries and from

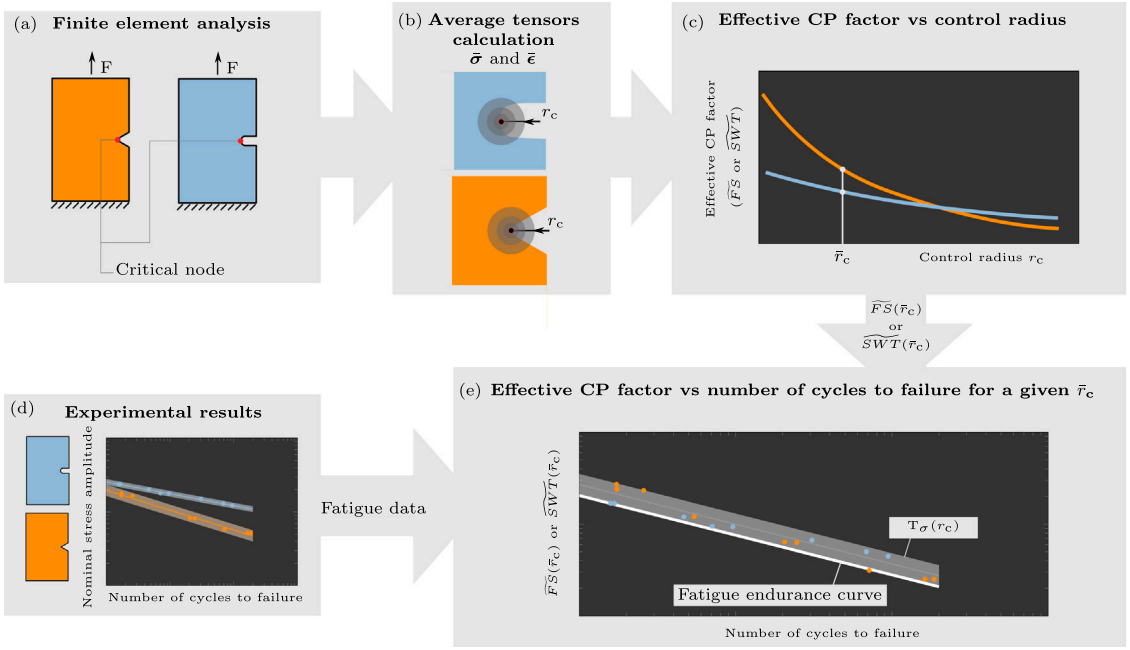

Fig. 1. Method workflow with reference to two specimen geometries: finite element simulations and identification of critical nodes (a), calculation of the averaged stress and strain tensors (b), calculation of the effective CP factor as a function of the control radius (c), use of data derived from experimental fatigue tests (d) for the evaluation of the effective CP values and endurance curve (e).

experimental campaigns conducted with different loading ratios and different loading conditions (e.g., tension, bending, torsion, combined in-phase and out-of-phase) can be used to cover a wide range of possible scenarios.

Deliberately, in the following sections, in order to check the capability of the proposed method, the reference endurance curve will be determined with reference only to two specimen geometries and a single loading conditions. The so obtained curve will then be employed to check the capability of the method in describing the failures of specimens made of the same material and having different geometries and being subjected to different loading conditions.

From the above analysis, it has to be observed that the ECP method mainly differentiate from other already presented methods, since it is based on a single concept, the critical plane, and for the fact that this concept preserves a tensorial description of the stress–strain field.

As a conclusion to this section, the operative implementation of the method is given, differentiating between two phases, namely calibration and assessment. The overall procedure was performed by means of a Matlab′ script, which is included as supplementary material to this article.

Calibration phase.

1. Perform a linear elastic FE analyses, under unitary load for, at least, two different notch geometries (Fig. 1a);
2. select the critical point, as the node having the maximum CP factor in the finite element models (according to FS or SWT);
3. define an array containing a range of control radii to be used, successively, (the range $r_c = [0, 0.7]$mm was chosen for this work);
4. calculate the average stress and strain tensor on a spherical volume or circular area centred on the critical node identified during step 2 for the pre-defined array of control radii of previous step 3 (Fig. 1b);
5. calculate the $\widetilde{FS}$ and $\widetilde{SWT}$ ECP factors, for a unitary load, for the pre-defined array of control radii by means of Eqs. (7)–(8), (Fig. 1c);
6. combine the experimental data (Fig. 1d) of nominal load (F) and number of cycles to failure (N_f) with the ECP factors evaluated at step 5 to derive the $\widetilde{FS}$ and $\widetilde{SWT}$ vs N_f for the pre-defined array of control radii (Fig. 1e);
7. generation of the fatigue scatter (T_{ECP}) curve vs r_c;
8. obtain the optimal control radius r_c and, thus, the best-fit endurance fatigue curves, $P_{10\%}$, $P_{50\%}$ and $P_{90\%}$, by finding the minimum of the scatter over the considered ranges of control radius.

Assessment phase.

1. Perform linear elastic finite element analyses under unitary load for all geometries to be analysed;
2. select the critical point as the node with the maximum CP factor in the finite element model (according to FS or SWT);
3. calculate the average stress and strain tensor on a spherical volume or circular area centred on the critical node identified during step 2, with the optimal control radius obtained during the calibration phase;
4. calculate, by means of Eqs. (7)–(8), the ECP $\widetilde{FS}$ and $\widetilde{SWT}$ factors under unitary load for the optimal value of the control radius r_c;
5. combine the experimental data of nominal load (F) and number of cycles to failure (N_f) with the ECP factors evaluated at step 4 to derive the $\widetilde{FS}$ and $\widetilde{SWT}$ vs N_f;
6. compare the data obtained in previous steps $1 - to - 5$ with the fatigue endurance curves obtained during the calibration phase.

3. Application to low carbon steel

In order to illustrate the practical application of the proposed method different notched specimens made of cold rolled low carbon steel En3B were selected from the literature. Specifically, two flat holed specimens, (Fig. 2a–b), one flat U-notched specimen (Fig. 2c), one flat V-notched specimen (Fig. 2d) with a thickness of 6 mm, referenced from Susmel and Taylor [24] and three cylindrical V-Notched specimens (Fig. 2e) having notch root radii (r_n) equal to 0.2 mm, 1.25 mm and 4 mm, referenced from Susmel and Taylor [62] were selected. Such specimens encompass uniaxial and multiaxial, in-phase and 90° out-of-phase tension and torsion fatigue test with load ratios of $R =$

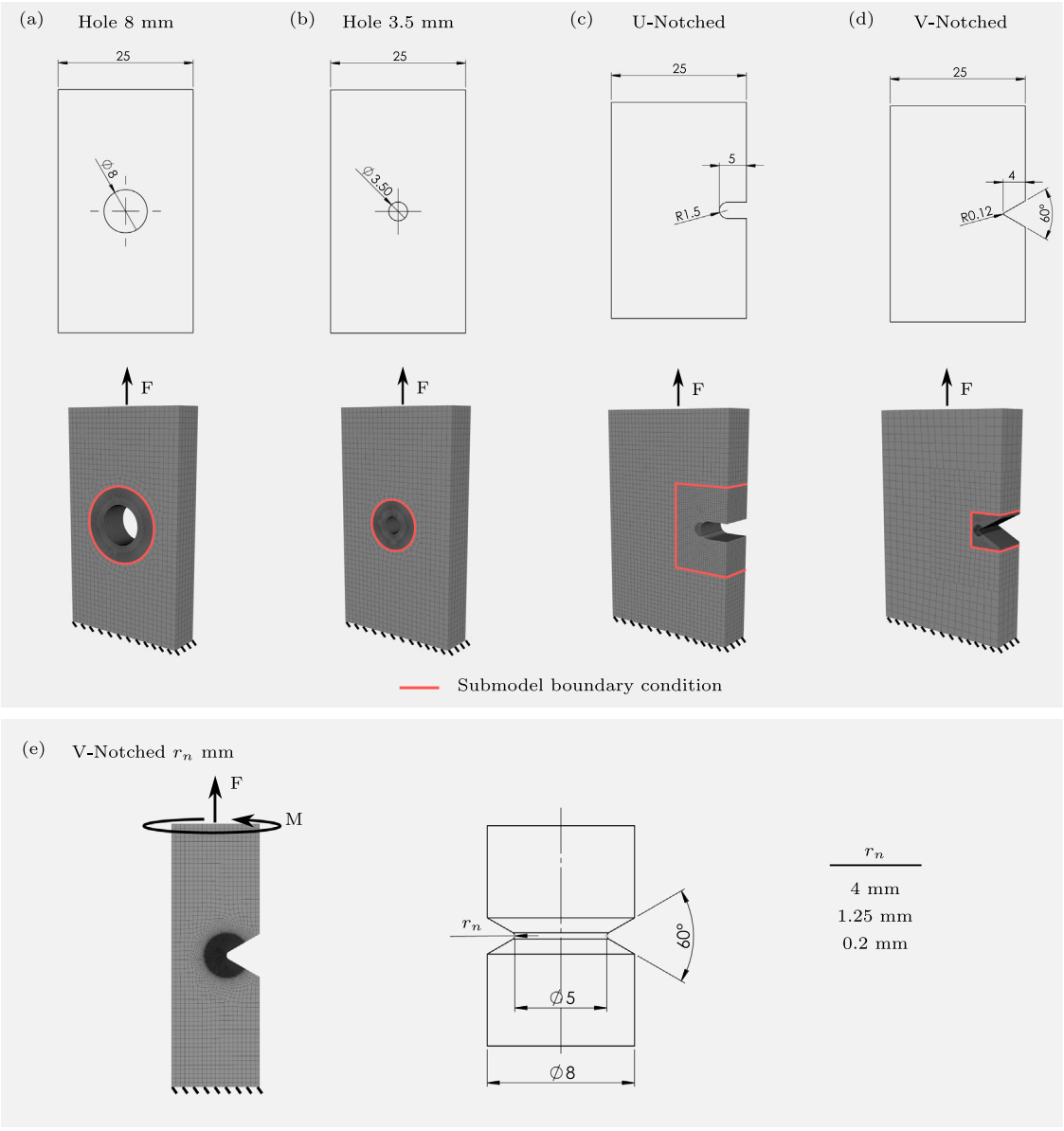

Fig. 2. Technical drawings and finite element models of the referenced geometries from Susmel and Taylor [24] (a)–(d) and Susmel and Taylor [62] (e): specimens with a central hole of 8 mm and 3.5 mm in diameter (a) and (b), specimen with a U-notch of 1.5 mm radius (c), specimen with a V-Notched of 0.12 mm radius (d) and V-Notched cylindrical specimens with a root radii ranging from 0.2 mm to 4 mm.

-1, $R = 0$ and $R = 0.1$. The chemical composition and material properties of En3B are given in Table 1. The specimen geometries were modelled and simulated using the Ansys software by checking the model fidelity with respect to the literature tensile and torsional concentration factors. Static structural analyses were performed using second order elements with linear elastic material properties and by employing the submodelling technique in the notch area, whenever necessary. The 3D and 2D finite element models were simulated by employing 20 nodes homogeneous structural solid (SOLID186) and 4 nodes structural solid (PLANE182) elements, respectively. The mesh was refined until numerical convergence of the numerical solution of stress and strain, over the control volume of radius r_c, occurred for all the investigated geometries (relative error on the stress concentration factors below 2%, as shown in Table 2). The mesh sizes presented in Table 2 were set throughout all the volume (i.e. for 3D models) or area (i.e. in 2D models) in which the factor averaging process is performed. It is worth noting that, the numerical convergence of the proposed ECP factor would be not as tight as the convergence of stress or strain components evaluated at each single node, due to the averaging process. Despite this, in this work, the convergence of the FE analysis was checked for the stress and strain nodal solution, ignoring the averaging process.

Table 1
Chemical composition, static and uniaxial fatigue properties of En3B low carbon steel.

Chemical composition of En3B steel (weight %)				
C	Mn	Si	P	S
0.16–0.24	0.50–0.90	max 0.35	max 0.05	max 0.05

Material properties of En3B [24]					
E (GPa)	ν_{el} (–)	ν_{pl} (–)	σ_{UTS} (MPa)	σ_y (MPa)	k
200	0.3	0.5	638.5	606.2	0.4

Just as an illustrative example, Fig. 3 presents the $\widetilde{FS}$ over r_c for all notched geometries of Fig. 2a–d. For each geometry, the ECP parameter

Table 2
Tensile (K_{ta}) and torsional (K_{t}) stress concentration factors and mesh sizes of notched specimens taken from [24,62].

Source	Geometry	FEM analysis		Literature		Dimensionality	Average mesh size (mm)
		K_{ta}	K_{tt}	K_{ta}	K_{tt}		
Susmel and Taylor [24]	V-Notched	16.52	–	16.2	–	3D	0.02
	U-Notched	6.21	–	6.1	–	3D	0.1
	Hole 8 mm	3.45	–	3.4	–	3D	0.1
	Hole 3.5 mm	3.13	–	3.1	–	3D	0.1
Susmel and Taylor [62]	V-Notched 4 mm	1.278	1.121	1.3	1.1	2D	0.04
	V-Notched 1.25 mm	1.776	1.317	1.8	1.3	2D	0.04
	V-Notched 0.2 mm	3.86	2.02	3.8	2.0	2D	0.01

has been evaluated at the node of the FE model having the maximum CP factor, under unitary tensile load and under a load ratio $R = -1$. The plots have been drawn for a maximum value of $r_c = 0.7$ mm, which is far beyond the optimal r_c value that will be obtained later on. In addition, the polynomial fit of the $\widetilde{FS}$ numerical data, obtained by a sixth degree polynomial, is also provided; the regression coefficient $R^2 > 99.9\%$ for all the investigated cases. The fitting polynomial is a convenient way to obtain the $\widetilde{FS}$ for different r_c values.

Similarly, Fig. 4 shows examples of the two curves (for the sake of simplicity, only the polynomial fits are shown) $\widetilde{\Delta\gamma}_{max}$ vs r_c and $\widetilde{\sigma}_n$ vs r_c, obtained under unitary load, which are necessary to compute the $\widetilde{FS}$ vs r_c, for any load value by Eq. (7). Two curves are provided for $\widetilde{\Delta\gamma}_{max}$ (i.e. for $R = 0.1$ and $R = -1$), while a single curve is given for $\widetilde{\sigma}_n$, since the simulation under unitary load presents the same maximum force for the cases of $R = 0.1$ and $R = -1$, while the shear strain range depends on the load ratio R. A similar procedure was carried out for the remaining geometries, not covered in the plots of Figs. 3 and 4 and for determining analogous parameter ($\widetilde{\Delta\epsilon}_{max}$ and $\widetilde{\sigma}_n$) with reference to the $\widetilde{SWT}$ ECP factor.

4. Results and discussion

By using the experimental data derived from Susmel and Taylor [24, 62], whose numerical values are given in Appendix, the master endurance curve for the investigated material and critical plane model can be obtained following the procedure illustrated in Fig. 1. Before that, in order to show all data, the von Mises equivalent stress amplitude has been plotted in Fig. 5 for all loading conditions and load ratios. As it can be observed, by using this representation, data appear dispersed and differences can be noticed due to the stress ratio R and to the loading conditions, with the multiaxial tests showing a higher fatigue strength. For each experimental data, the $\widetilde{FS}$ ECP and $\widetilde{SWT}$ ECP parameters described in Section 2 can be obtained as a function of the control radius r_c. By taking account of the experimental number of cycle to failures, the fatigue curves $\widetilde{FS}$ vs N_f and $\widetilde{SWT}$ vs N_f are then obtained, for any given control radius, as well.

The optimal control radius of the averaging volume was then determined by minimizing the fatigue scatter index T_{ECP}, between the $P_{10\%}$ and $P_{90\%}$ fatigue endurance curves. The scatter is evaluated with respect to the best fit interpolating power law, obtained considering all processed data; the slope of the best fit line (in log–log scale) was obtained by the fitting procedure, as well.

To this aim, deliberately, the specimen geometries having the most severe and least severe notch effect, namely the V-Notched and Hole 8 mm, were employed, all the other data, being subsequently used to validate the model capability in calculating the expected fatigue endurance. High cycle fatigue data (i.e. with $N_f > 3 \times 10^4$) were used for the minimization of the scatter; very few experimental data, related to high stressed specimens, were intentionally not included to avoid any possible effect due to plasticity.

The variation of T_{ECP} vs r_c is presented in Fig. 6 for the two critical plane models investigated. Figs. 6a–b report the T_{ECP} vs r_c, according to the $\widetilde{FS}$ and $\widetilde{SWT}$ models, respectively, obtained from analysing the V-Notched and Hole 8 mm experimental data with load ratio $R = 0.1$ and $R = -1$. As it can be observed, all the plots of the scatter index vs control radius have a minimum, which identify the optimum value of the control radius. The single-variable optimization analysis yields a minimum $r_c^{FS} = 0.20$ mm and $r_c^{SWT} = 0.25$ mm for the $\widetilde{FS}$ ECP and for the $\widetilde{SWT}$ ECP parameter, respectively. It is interesting to note that the same control radii are obtained by analysing solely data with load ration of $R = -1$, as presented in Figs. 6c–d. This means that, for the selected material, only two experimental data sets are sufficient for the calibration procedure, namely V-Notched and Hole 8 mm under $R = -1$. This can be explained by the fact that the employed critical plane factors (i.e. both FS and SWT) inherently take into account the mean stress (i.e. different load ratios) through the maximum normal stress parameter σ_n acting on the critical plane. The possibility to determine fatigue lives at different load ratios, based on the experimental fatigue curve obtained with a single load ratio represents a significant simplification for the method to be applied. In order to further check the robustness of the control radius, the calibration procedure was repeated for 26 different combinations of data related to uniaxially loaded geometries with different loading ratios presented in Fig. 2a–d (see Table 3); more in details, the first 8 data are obtained based on possible combination of 2 geometries, varying the load ratio R, while the other 18 data are obtained by using data belonging to 4 different geometries, varying the load ratio. The last two columns give the control radius and the slope coefficient of the fatigue curve, obtained by the best fitting procedure. It can be concluded that the optimal control radius is stable, showing a mean value of 0.204 mm and a standard deviation of 0.016 mm, demonstrating the robustness of the r_c value as a material constant. The slope coefficient appears stable, as well, having a standard deviation which is about 10% of the mean value.

Once the optimal control radius has been determined for the selected material and ECP factor, the endurance curves can be obtained. These are shown in Fig. 7, for both, $\widetilde{FS}$ and $\widetilde{SWT}$ ECP factors. These curves were obtained by using experimental data of the V-Notched and Hole 8 mm specimens for a single load ratio, i.e. $R = -1$, and considering data with $N_f > 3 \times 10^4$.

The following Fig. 8 shows all the other experimental data points derived from the remaining geometries, processed according to the described ECP method. Fig. 8a provides data of $\widetilde{FS}$ vs N_f together with the endurance curves obtained during the calibration procedure of Fig. 7a, while Fig. 8b reports data of $\widetilde{SWT}$ vs N_f together with the endurance curves obtained during the calibration procedure of Fig. 7b. The fatigue scatter derived from the prevision data are given in the Figures.

It is interesting to observe that the $\widetilde{SWT}$ scatter is significantly larger than the one obtained by the $\widetilde{FS}$ parameter, 1 : 4.55 and 1 : 1.77, respectively. This can be attributed to the fact that, the shear cracking mechanism typical of the analysed material is better described by the *Fatemi-Socie* parameter. This difference is also noticeable by comparing the fatigue scatter of $\widetilde{SWT}$ and $\widetilde{FS}$, with respect to the fatigue scatters derived from every single dataset, as shown in Table 4.

With reference to multiaxial data, it is worth noting that the $\Delta\gamma_{max}$, necessary to define the $\widetilde{FS}$, has been evaluated using the Minimum Circumscribed Circle (MCC) method for all cases except for the 90° out-of-phase loading. In fact, it is known that the MCC method, similarly to

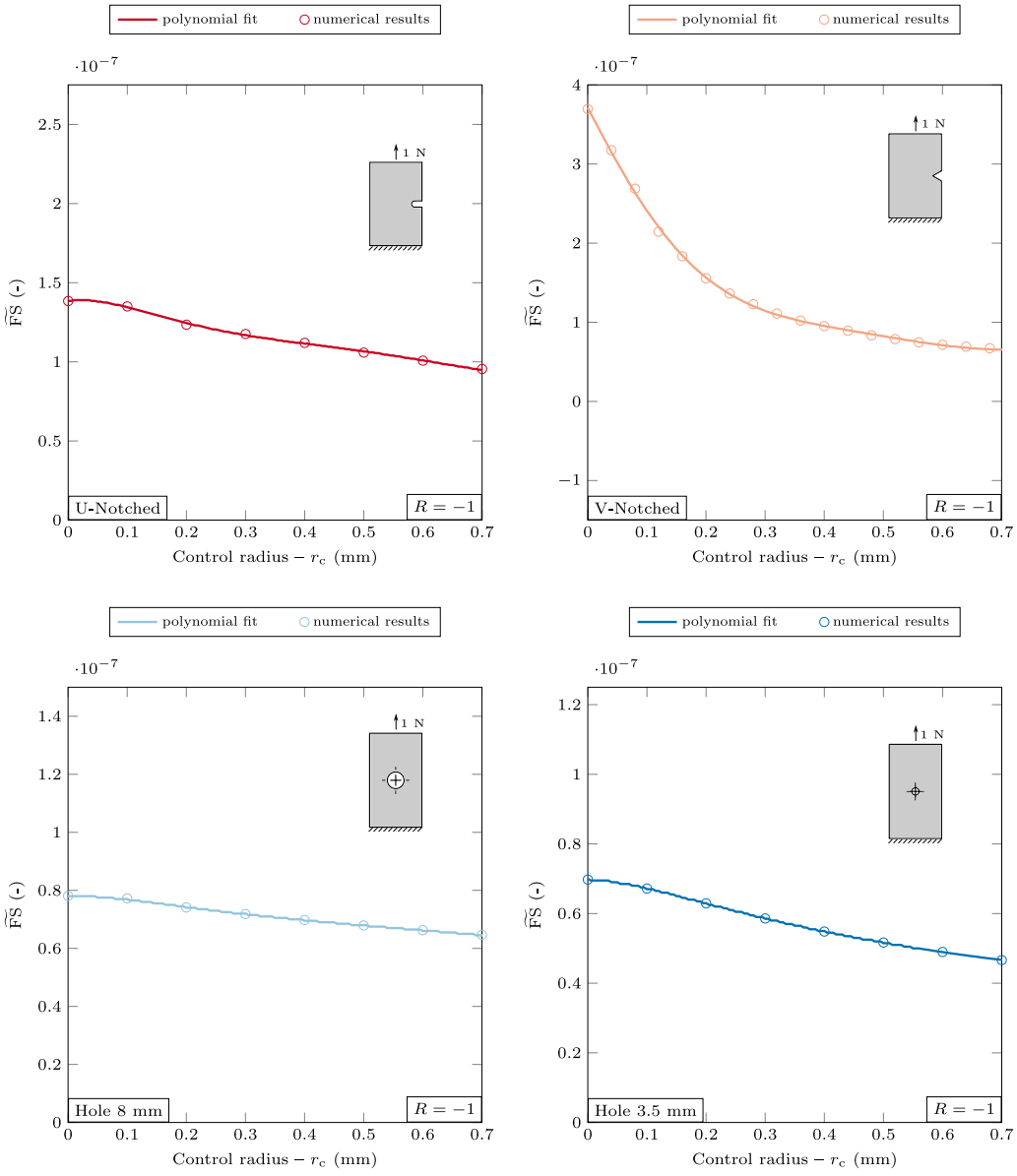

Fig. 3. Evolution of the $\widetilde{FS}$ ECP factor obtained under unitary load for varying control radius for different notched geometries considered; both data from finite element simulation and polynomial fit with $R^2 > 99.9\%$ are reported.

other methods such as the Longest Chord (LC) and Longest Projection (LP) cannot truly differentiate between proportional loading and non-proportional loading. For this reason, in the case of the 90° out-of-phase loading the parameter $\Delta\gamma_{max}$ was computed as the Maximum Path Half Perimeter (MPHP) obtained by following the γ vector on each plane orientation. This was inspired by other works (e.g., Mei et al. [70]), with the intention to consider the effect of load phase shift and to obtain more accurate results. The difference between the MPHP and the MCC method is presented in Fig. 9, where only the 90° out-of-phase multiaxial results are shown. A significant difference in $\widetilde{FS}$ can be observed for all the notched geometries, with data interpreted by the MPHP method providing a higher $\widetilde{FS}$ values, i.e. a shorter life, for a given reference endurance curve.

From the analysis of Fig. 8, it can be observed that the $\widetilde{FS}$ ECP factor, evaluated with the control radius r_c^{FS} determined solely on the basis of two geometries and simple axial loading, appears capable of describing with fully satisfactory accuracy the fatigue lives for all the tests, considering the different geometries and loading conditions, including torsion and both in-phase and out-of-phase multiaxial loading.

The $\widetilde{SWT}$ ECP appears to be less accurate for this kind of material, and the analysed data show a larger dispersion; in particular, data relative to V-notched specimens under multiaxial loading conditions show a relatively large distance from the best fit endurance curve, obtained for the reference geometries and loading case, which were used to determine the reference endurance curve and control radius.

Similar considerations can be drawn with reference to Fig. 10, showing the expected vs experimental fatigue lives for all the experimental data that were analysed (the calibration data have been also included in these graphs). In this case, the expected lives were determined on the basis of the $P_{50\%}$ reference endurance curve (i.e. best fit) of Fig. 7. It can be observed that the expected fatigue lives are equally distributed on both conservative and non-conservative sides in case of $\widetilde{FS}$ formulation. On the contrary, expected fatigue lives are more distributed on the non-conservative side in case of $\widetilde{SWT}$ formulation. In the case of FS model,

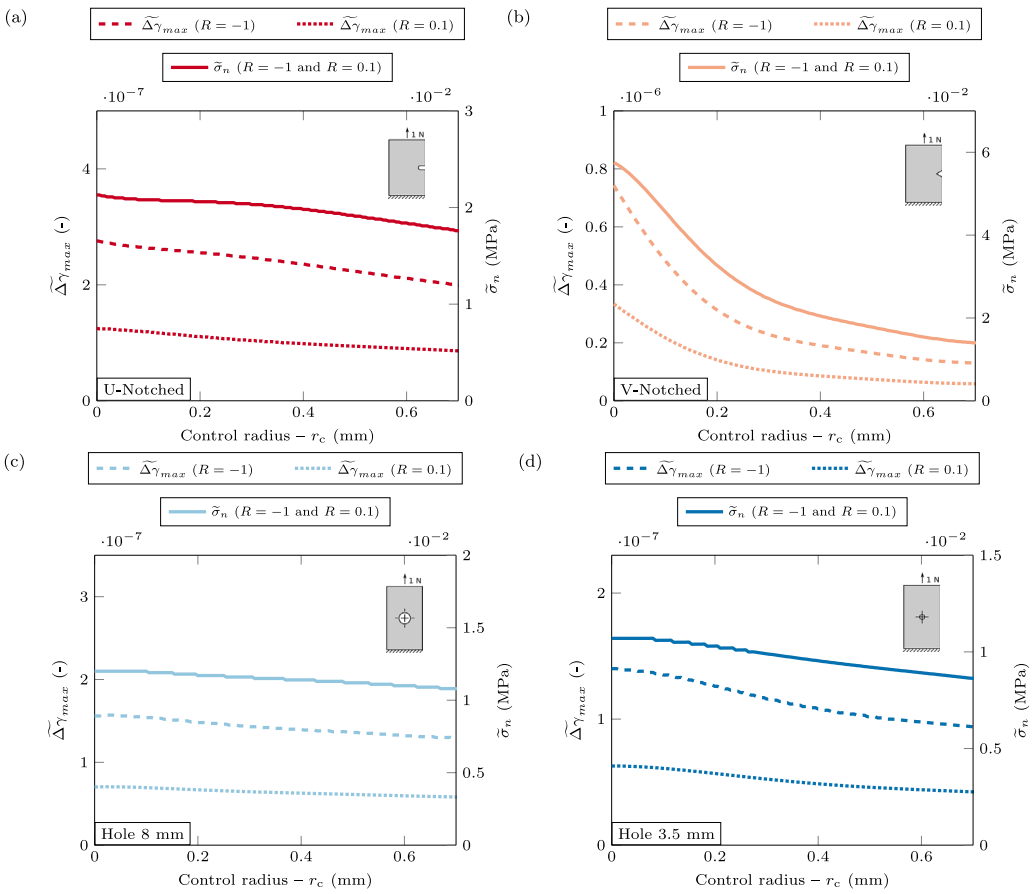

Fig. 4. Polynomial fit with $R^2 > 99.9\%$ of the averaged $\widetilde{\Delta\gamma}_{max}$ and $\widetilde{\sigma}_n$ factors obtained under unitary load for varying control radius for the notched geometries retrieved from Susmel and Taylor [24].

Table 3
Evaluation of the control radius r_c^{FS} and fatigue curve slope m for several combinations of uniaxially loaded geometries and load ratios presented in Fig. 2a–d.

Geometry$_1$	R_1	Geometry$_2$	R_2	Geometry$_3$	R_3	Geometry$_4$	R_4	r_c^{FS}	m
U-Notched	−1	V-Notched	−1					0.19	3.62
U-Notched	0.1	V-Notched	0.1					0.18	3.12
Hole 8 mm	−1	V-Notched	−1					0.20	4.29
Hole 8 mm	0.1	V-Notched	0.1					0.23	3.39
Hole 3.5 mm	0.1	U-Notched	0.1					0.19	3.85
Hole 3.5 mm	−1	U-Notched	−1					0.19	4.39
Hole 3.5 mm	−1	V-Notched	−1					0.19	4.48
Hole 3.5 mm	0.1	V-Notched	0.1					0.19	3.22
Hole 3.5 mm	−1	V-Notched	−1	Hole 3.5 mm	0.1	V-Notched	0.1	0.20	3.69
Hole 3.5 mm	−1	V-Notched	−1	Hole 3.5 mm	0.1	U-Notched	0.1	0.21	4.18
Hole 3.5 mm	−1	V-Notched	−1	Hole 3.5 mm	0.1	V-Notched	0.1	0.20	3.69
U-Notched	−1	V-Notched	−1	Hole 8 mm	−1	Hole 3.5 mm	−1	0.20	4.10
U-Notched	0.1	V-Notched	0.1	Hole 8 mm	0.1	Hole 3.5 mm	0.1	0.20	3.52
Hole 8 mm	−1	V-Notched	−1	Hole 8 mm	0.1	V-Notched	0.1	0.21	3.73
Hole 3.5 mm	−1	V-Notched	−1	Hole 8 mm	0.1	V-Notched	0.1	0.21	3.80
Hole 3.5 mm	−1	V-Notched	−1	Hole 8 mm	0.1	U-Notched	0.1	0.23	4.42
U-Notched	−1	V-Notched	−1	U-Notched	0.1	V-Notched	0.1	0.18	3.40
U-Notched	−1	V-Notched	−1	U-Notched	0.1	Hole 8 mm	0.1	0.24	3.68
U-Notched	−1	V-Notched	−1	U-Notched	0.1	Hole 3.5 mm	0.1	0.21	3.62
Hole 8 mm	−1	V-Notched	−1	U-Notched	0.1	V-Notched	0.1	0.19	3.45
Hole 8 mm	−1	V-Notched	−1	U-Notched	0.1	Hole 8 mm	0.1	0.23	4.17
Hole 8 mm	−1	V-Notched	−1	U-Notched	0.1	Hole 3.5 mm	0.1	0.22	3.95
Hole 3.5 mm	−1	V-Notched	−1	U-Notched	0.1	V-Notched	0.1	0.19	3.57
U-Notched	−1	V-Notched	−1	V-Notched	0.1	Hole 8 mm	0.1	0.20	3.50
U-Notched	−1	V-Notched	−1	V-Notched	0.1	Hole 3.5 mm	0.1	0.19	3.39
Hole 8 mm	−1	V-Notched	−1	V-Notched	0.1	Hole 3.5 mm	0.1	0.20	3.57
				Standard deviation				0.016	0.380
				Average				0.20	3.76

the vast majority of results fall within a scatter band of factor 5 (90%) and a significant percentage within a band of factor 3 (74%). The use of the ECP approach has the advantage of encompassing aspects hardly accountable with other methods, such as variable load ratios, load

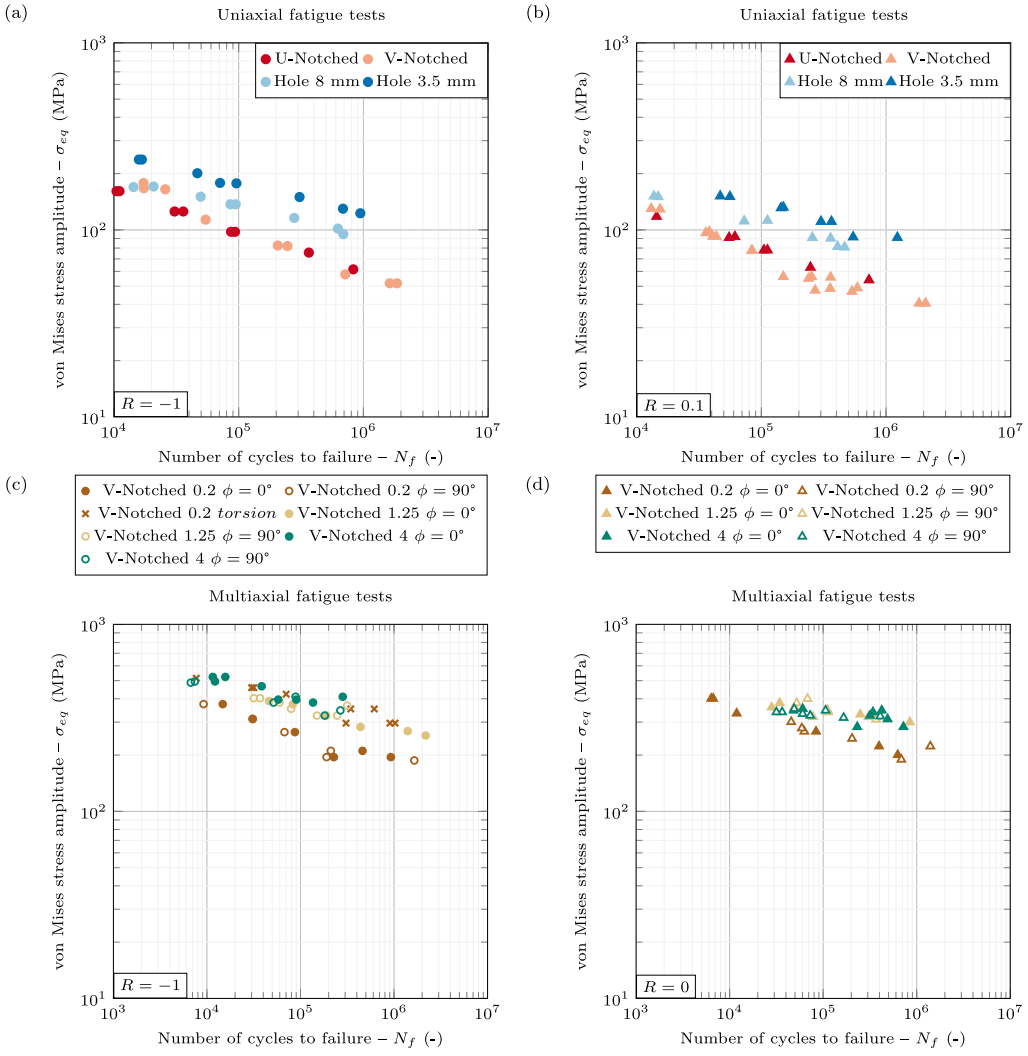

Fig. 5. von Mises equivalent stress amplitude, evaluated starting from experimental fatigue results, taken from Susmel and Taylor [24,62] for notched geometries tested under uniaxial (a)–(b) and multiaxial (c)–(d) in-phase and out-of-phase loading with different loading ratios $R = -1$, $R = 0.1$ and $R = 0$.

multiaxiality and non-proportionality. Specifically for FS applied to the ECP approach the σ_n accounts for the change in load ratio (i.e. mean stress variation), the γ path and critical plane orientation accounts for the load non-proportionality and the combination of γ and σ_n accounts for the multiaxiality. Overall, the assessment of the fatigue life seems to be in line with other methods, namely NSA, TCD and SED.

By looking at the expected fatigue lives, it is noticeable how the $\widetilde{\text{FS}}$ formulation better describes the occurred failures in comparison to the $\widetilde{\text{SWT}}$ parameter, for the selected ductile material. As already stated, this can be attributed to the fact that the FS parameter better describe the fatigue failure process for the analysed material. The SWT formulation is expected to fit better data relative to materials prone to brittle fracture, promoted by normal stresses and strains.

The optimal control radii obtained by the two investigated critical plane methods are somewhat different. The control radius found for SWT is slightly greater than that obtained for FS, $r_c^{\text{SWT}} = 0.25\,\text{mm}$ and $r_c^{\text{FS}} = 0.20\,\text{mm}$ respectively. This has to be attributed to the different formulation of the fatigue parameter similarly to what happens if other formulations are used (e.g. switching from SED to TCD).

One of the most promising result is that, at least for the analysed material, the proposed ECP methodology allows for unifying, within reasonable scatter, fatigue data related to notched geometries with different severities and different loading conditions, by using a single constant parameter, which only depends on the material type. Additional investigation related to different materials have to be carried out to check if this result can be generalized.

It is interesting to observe also that the optimal control radius seems to be insensitive to mean stress variation, for both CP formulations; this can be attributed to the fact that the mean stress effect is somewhat included within the considered CP formulations, through the maximum normal stress.

In other words, a single r_c value yields promising results for a large variety of notch geometries and loading conditions and this is particularly interesting for practical applications, e.g. in the industry sector. In the authors' opinion this is due to the fact that the ECP preserves a tensorial description of the stress–strain field, allowing to intrinsically take account of complex loading conditions. On the contrary, methods based on scalar parameters need different calibrations in relation to mean stress variation and for complex stress state histories; Susmel and Taylor [62] reinterpreted MWCM in terms of the TCD PM by employing four different calibration fatigue curves, two of them used to calibrate the MWCM, one used to calibrate the mean stress sensitivity and the last one needed to determine the material characteristic length as a function of the number of cycles to failure; Pedranz et al. [52] introduced correction factors for mean stress effect and for non proportional loading modes.

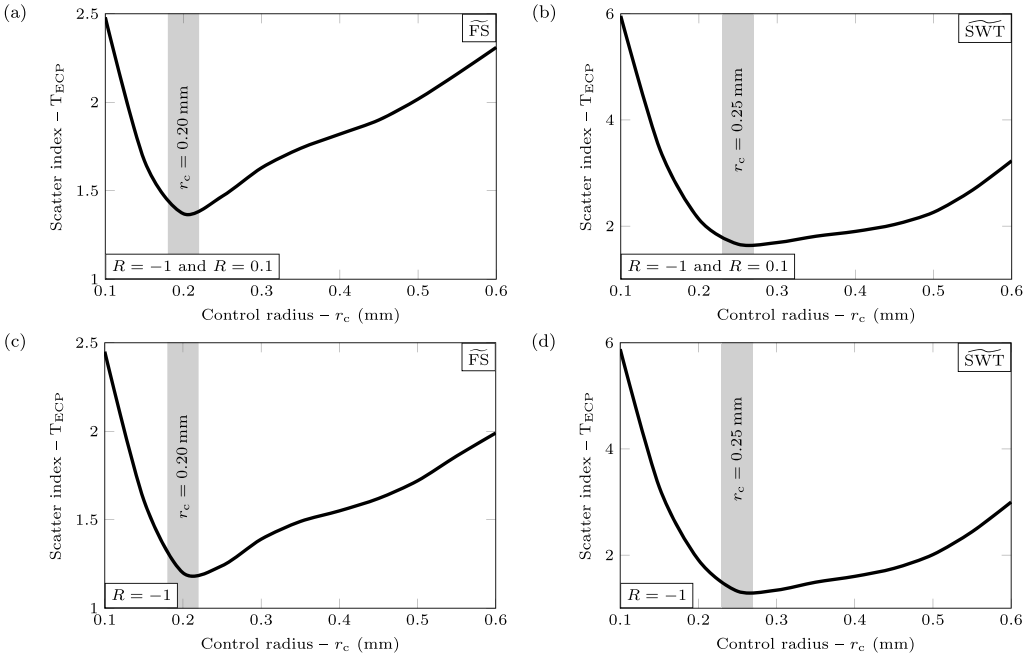

Fig. 6. Fatigue scatter variation curve for the experimental data points with $N_f > 3 \times 10^4$ of V-Notched and Hole 8 mm specimens derived from [24], under loading ratios of $R = -1$ and $R = 0.1$ for the FS model (a) and SWT model (b), and loading ratio of $R = -1$ for the FS model (c) and SWT model (d).

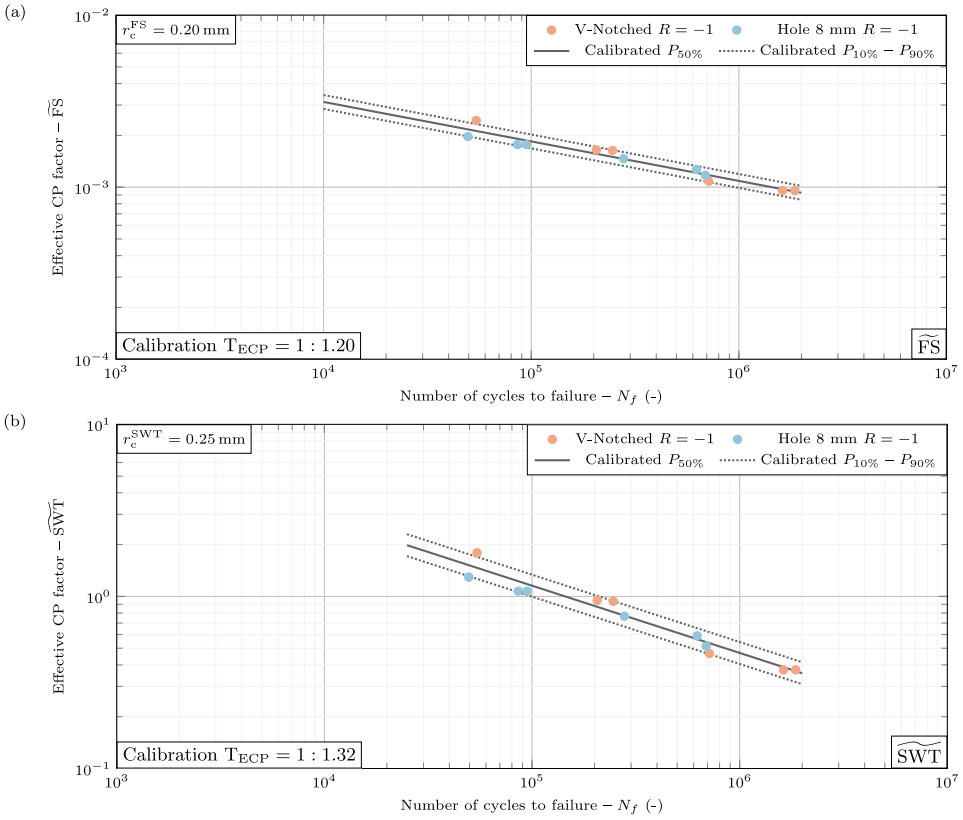

Fig. 7. Calibrated endurance curves obtained through an experimental data set of tensile fatigue test derived from [24] for a control radius of $r_c = 0.20$ mm in case of FS model (a) and for a control radius of $r_c = 0.25$ mm in case of SWT model (b).

In order to benchmark the goodness of the proposed ECP method against traditional methods, the error on the fatigue assessment was determined by the parameter defined in [47]:

$$E_N = \log_{10}\left(\frac{N_f}{N_{f,e}}\right) \tag{9}$$

where N_f and $N_{f,e}$ represent the experimental and expected fatigue lives, respectively.

The Probability Density Function (PDF) distributions of E_N, for the different literature data analysed, are given in Figs. 11. The uniaxial experimental data referenced in this paper originally underwent

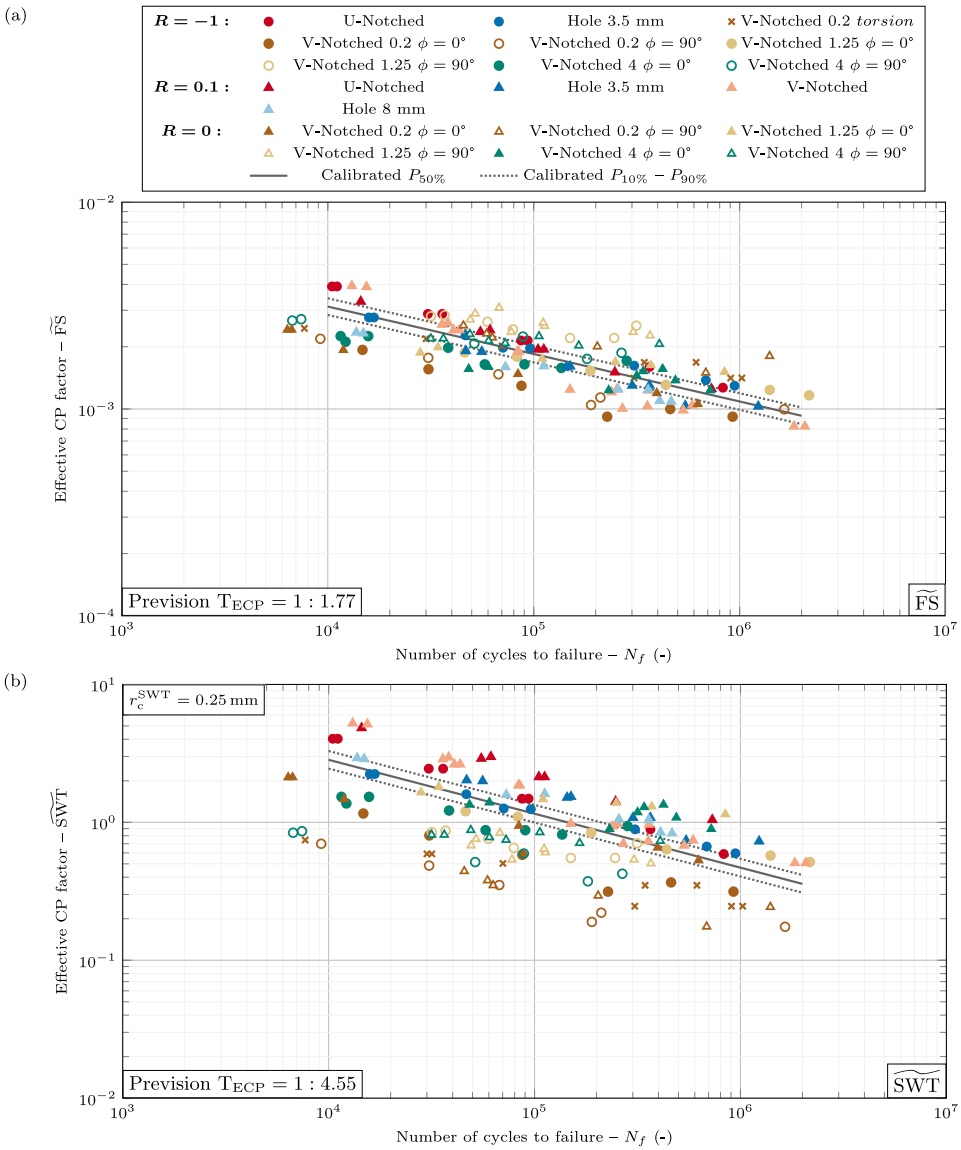

Fig. 8. Effective CP factors $\widetilde{FS}$ vs number of cycles to failure (a) and $\widetilde{SWT}$ vs number of cycles to failure (b) for different notched geometries derived from [24,62]; the fatigue data points represent uniaxial and multiaxial in-phase and out-of-phase loading conditions, together with the calibrated endurance curves $P_{10\%}$, $P_{50\%}$ and $P_{90\%}$ of Fig. 7.

evaluation through the TCD PM, LM and AM as reported in Susmel and Taylor [24], while the multiaxial experimental data were assessed by the Modified Wohler Curve Method (MWCM), within the TCD PM framework as reported in Susmel and Taylor [62] and by the SED method as presented by Hu et al. [47].

In details, Fig. 11a reports the statistical distribution for uniaxial data while Fig. 11b that for the multiaxial data. Assuming that the data follow a normal distribution, the standard deviation σ is a measure of the dispersion of the expected lives, while the mean value μ indicates how the distribution is skewed toward the conservative (i.e. positive μ) or non-conservative side (i.e. negative μ); positive mean value indicates shorter expected lives if compared to experimental data and negative mean value indicates longer expected lives if compared to experimental data. The data considered are also presented in Fig. 12, which reports the expected vs experimental number of cycles to failure for all datasets considered with the exception of $\widetilde{SWT}$ ECP.

Limited to the ECP method, it can be seen that, for the analysed material, the $\widetilde{FS}$ method performs better, providing lower mean and standard deviation than $\widetilde{SWT}$. Compared with traditional methods, $\widetilde{FS}$ yields results that are fully consistent in both uniaxial and multiaxial dataset, exhibiting a 38.6% decrease in standard deviation compared with the SED method and an appreciable decrease of the mean value, if compared with the MWCM method combined with TCD PM method, resulting in a more balanced distribution of expected lives. To this regard, however, it is worth noting that, the MWCM method combined with TCD PM method of Fig. 11b necessitates four distinct calibration fatigue curves (refer to Susmel and Taylor [62]), while the SED method, applied to multiaxial fatigue test, requires the knowledge of the radius of the control volume under Mode I and Mode III loading in addition to the weighting parameter accounting for varying load ratios. On the contrary, the proposed ECP method achieves a comparable fatigue scatter employing a single constant calibration parameter r_c, which can be easily derived on the basis of two experimental fatigue data set, obtained for two different notch geometries, both under loading ratio $R = -1$.

5. Conclusions

In the present work a novel approach for the fatigue assessment, based on the so called Effective Critical Plane, was proposed. This approach has the intention to join the critical plane hypothesis (preferred crack orientations) with the stress averaging concept (small process

Table 4
Fatigue scatter derived by the implementation of $\widetilde{\text{FS}}$ and $\widetilde{\text{SWT}}$ on all the analysed datasets.

		$\widetilde{\text{FS}}$ calibrated with $r_c^{FS} = 0.20$ mm	$\widetilde{\text{SWT}}$ calibrated with $r_c^{SWT} = 0.25$ mm
Dataset	R	T_{ECP}	T_{ECP}
		Single dataset	
U-Notched	−1	1.074	1.111
V-Notched	−1	1.132	1.225
Hole 3.5 mm	−1	1.060	1.101
Hole 8 mm	−1	1.056	1.106
V-Notched 0.2 *torsion*	−1	1.194	1.426
V-Notched 0.2 $\phi = 0°$	−1	1.271	1.522
V-Notched 0.2 $\phi = 90°$	−1	1.326	1.650
V-Notched 1.25 $\phi = 0°$	−1	1.101	1.178
V-Notched 1.25 $\phi = 90°$	−1	1.189	1.364
V-Notched 4 $\phi = 0°$	−1	1.201	1.385
V-Notched 4 $\phi = 90°$	−1	1.165	1.330
U-Notched	0.1	1.098	1.156
V-Notched	0.1	1.391	1.598
Hole 3.5 mm	0.1	1.150	1.266
Hole 8 mm	0.1	1.106	1.187
V-Notched 0.2 $\phi = 0°$	0	1.131	1.217
V-Notched 0.2 $\phi = 90°$	0	1.262	1.508
V-Notched 1.25 $\phi = 0°$	0	1.066	1.108
V-Notched 1.25 $\phi = 90°$	0	1.202	1.355
V-Notched 4 $\phi = 0°$	0	1.251	1.468
V-Notched 4 $\phi = 90°$	0	1.095	1.162
		Combined datasets	
Calibration dataset	−1	1.202	1.318
Prevision dataset	−1, 0.1 and 0	1.773	4.549

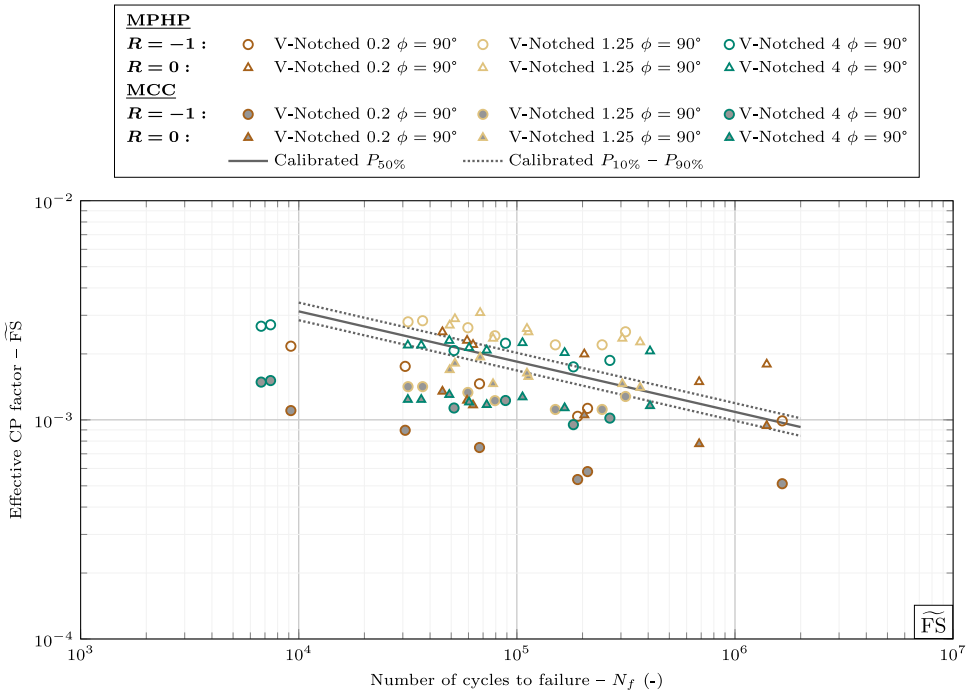

Fig. 9. Effective CP factor $\widetilde{\text{FS}}$ vs number of cycles to failure for two different $\Delta\gamma_{max}$ calculation methods, namely MPHP and MCC; the reference endurance curve already shown in Fig. 8. is also shown.

volume where fatigue cracks originate). The *Fatemi-Socie* and *Smith-Watson-Topper* critical plane factors have been used to explore the applicability of the proposed approach. Experimental fatigue data taken from the literature and relative to low carbon steel specimens featuring various notches and loading conditions were employed. Two notched geometries under fully reversed uniaxial loading condition were used, firstly, to determine the control radius of the averaging process, by a best fitting procedure. All the other experimental data, relative to different notches and loading conditions, including in-phase and out-of-phase multiaxial loading, were then employed to validate the method's capability to accurately describe the observed fatigue lives. On the basis of the performed analysis the following main conclusions can be drawn:

- as opposite to the vast majority of the methods based on scalar parameters, such as SED and TCD, the use of the CP concept preserves the full tensorial description of the stress field and this allows to take account, efficiently, of mean stress variation and of different loading modes, including complex multiaxial out of phase conditions;

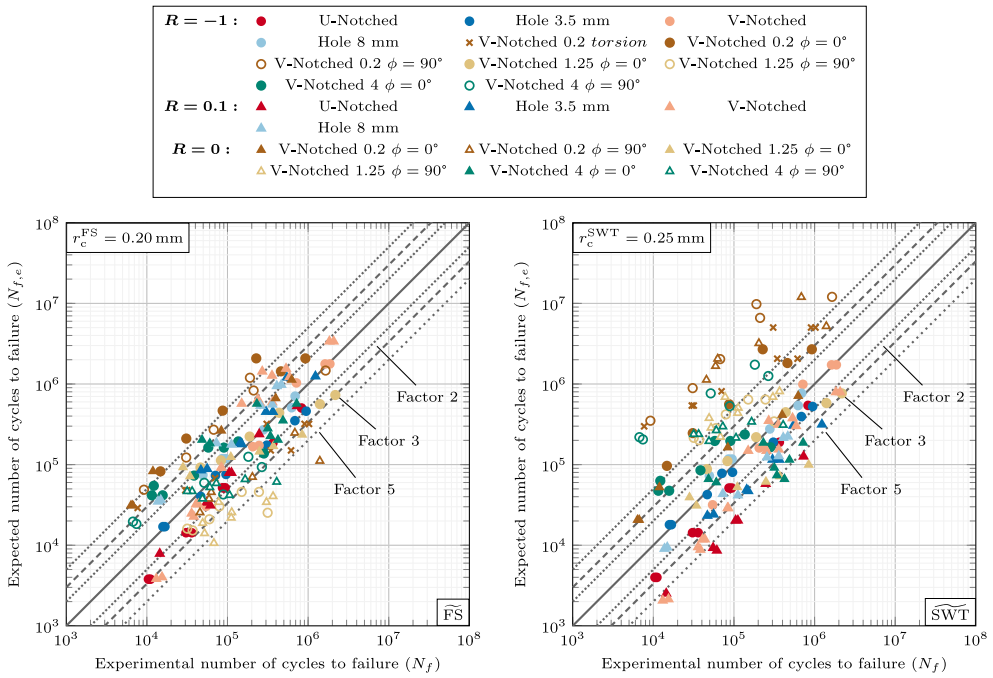

Fig. 10. Expected vs experimental number of cycles to failure obtained for different notched geometries and loading conditions derived from [24,62] by implementing $\widetilde{FS}$ and $\widetilde{SWT}$ CP factors.

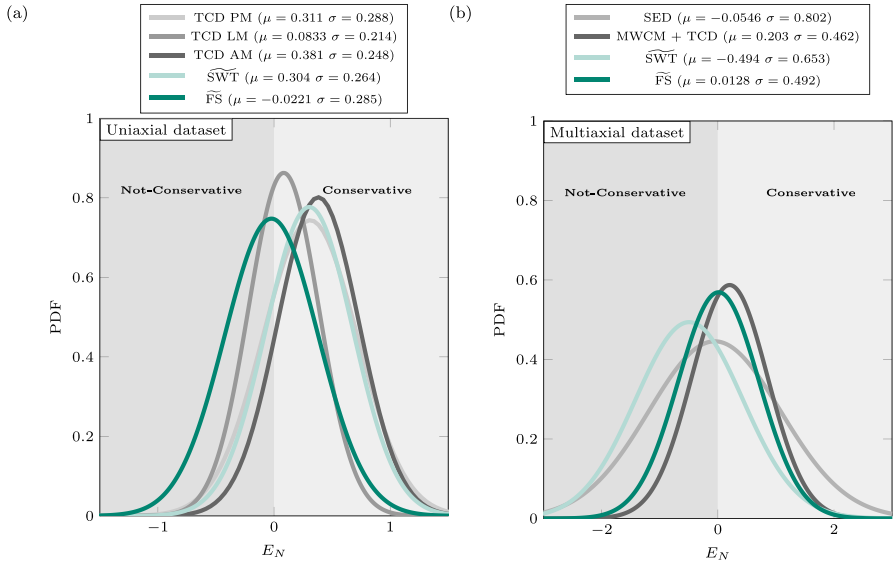

Fig. 11. Probability density function in the case of a normal distribution of the parameter E_N defined in Eq. (9), for uniaxial experimental data (a) and multiaxial experimental data (b) processed by means of different methods.

- for the analysed material (i.e. low carbon steel), the proposed methodology proved capable of providing a single master endurance curve, describing with a fully satisfactory agreement, at least for one ECP parameter, experimental results obtained with different notch geometries, different loading modes and different load ratios;
- the method make use of a single material dependent parameter, i.e. the control radius r_c, used in the averaging process, which, at least for the analysed material, was shown to have minimal variation among different calibration datasets and, ultimately, that can be calibrated using just two sets of fatigue experimental data, related to a single load ratio R=-1; this seems to be particularly attractive, especially for the industry;
- for the selected material, the $\widetilde{FS}$ ECP factor appears to better describe the fatigue data, in comparison to the $\widetilde{SWT}$ ECP parameter; this is related to the shear cracking phenomenon, typical for mild steel;
- the analysis of literature data with simple linear elastic FE simulation and the $\widetilde{FS}$ ECP parameter provided a fairly good estimate of the fatigue lives of notched low-carbon steel specimens under uniaxial and multiaxial in-phase and out-of-phase loading, with most of the results (i.e. 74%) falling within a scatter band of 3;
- in relation to the analysed data, the proposed method appears to be advantageous with respect to other literature methods, which require the calibration of several parameters, especially when dealing with multiaxial non-proportional loading conditions, thus requiring longer experimental investigations;
- the obtained results seem promising for the application of the proposed methodology to completely general (even complex 3D)

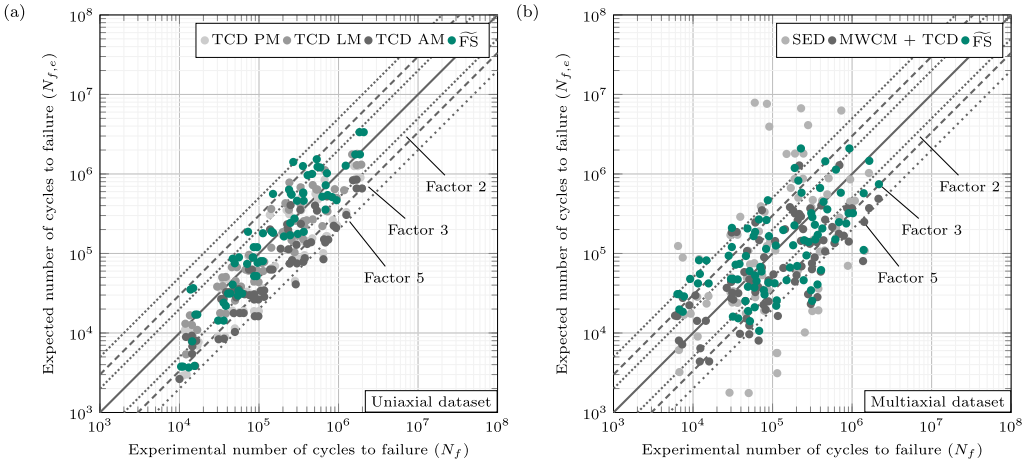

Fig. 12. Expected vs experimental number of cycles to failure for uniaxial experimental data (a) and multiaxial experimental data (b) processed by means of different methods.

geometries and loading condition, with the aid of FE analysis, exploiting the recent computationally efficient strategies (i.e. closed form solutions) for CP factors evaluation developed by the authors.

The integration and merging of already established methodologies represents a significant step in fatigue assessment. By bridging the gap between theoretical advancements and practical validation through experimental results, this approach showcases a promising potential for real-world applications, for the assessment of the fatigue life of notched components subjected to complex loading conditions.

Future steps will include additional analyses of fatigue data for different geometries, different class of materials, different critical plane factors and the application to real components to determine if the obtained results can be generalized.

CRediT authorship contribution statement

A. Chiocca: Writing – original draft, Visualization, Validation, Software, Methodology, Investigation, Formal analysis, Data curation, Conceptualization. **F. Frendo:** Writing – review & editing, Supervision, Resources, Project administration, Funding acquisition, Formal analysis, Conceptualization.

Declaration of competing interest

The authors declare the following financial interests/personal relationships which may be considered as potential competing interests: Francesco Frendo reports financial support was provided by Ministero dell'Universitá e della ricerca. If there are other authors, they declare that they have no known competing financial interests or personal relationships that could have appeared to influence the work reported in this paper.

Data availability

Data will be made available on request.

Acknowledgements

Financed by the European Union - NextGenerationEU (National Sustainable Mobility Center CN00000023, Italian Ministry of University and Research Decree n. 1033 - 17/06/2022, Spoke 11 - Innovative Materials & Lightweighting). The opinions expressed are those of the authors only and should not be considered as representative of the European Union or the European Commission's official position. Neither the European Union nor the European Commission can be held responsible for them.

Appendix. Fatigue data

See Tables A.5–A.8.

Supplementary data

A Matlab® script which implements the ECP $\widetilde{FS}$ algorithm reported in the article has been uploaded to a GitHub repository: https://github.com/achiocca1/ECP. In addition, the data shown in Figs. 7, 8 and 10 have been uploaded to an online repository with the following doi: 10.5281/zenodo.12721131.

Table A.5
Uniaxial experimental data of Fig. 5 obtained from Susmel and Taylor [24] for a load ratio of $R = -1$.

Uniaxial fatigue tests from Susmel and Taylor [24]			
Geometry	R	N_f	σ_a (MPa)
U-Notched	−1	10 480	161.1
		11 078	161.1
		30 640	125.5
		35 970	125.5
		86 861	97.7
		93 534	97.7
		365 413	75.6
		829 687	61.5
V-Notched	−1	17 274	178.1
		17 379	167.2
		25 790	165.0
		54 368	113.5
		205 936	82.5
		246 267	82.0
		715 477	57.8
		1 624 734	51.9
		1 860 848	51.8
Hole 8 mm	−1	14 355	169.4
		20 784	170.6
		49 582	150.6
		85 835	137.1
		94 738	137.1
		278 724	115.9
		625 161	101.6
		689 936	94.9
Hole 3.5 mm	−1	15 851	237.8
		16 756	237.8
		46 635	200.9
		70 922	178.4
		95 947	177.4
		307 738	149.9
		685 982	129.8
		945 291	122.7

Table A.6
Uniaxial experimental data of Fig. 5 obtained from Susmel and Taylor [24] for a load ratio of $R = 0.1$.

Uniaxial fatigue tests from Susmel and Taylor [24]			
Geometry	R	N_f	σ_a (MPa)
U-Notched	0.1	14 462	118.0
		55 131	91.4
		61 381	92.8
		104 975	78.4
		111 960	78.4
		247 744	63.9
		730 011	54.8
V-Notched	0.1	13 085	130.0
		15 426	129.1
		35 884	96.4
		38 272	97.8
		40 816	92.3
		43 532	92.3
		83 481	77.5
		84 685	77.5
		150 071	56.2
		269 839	47.6
		238 975	55.0
		253 069	56.2
		359 389	55.8
		356 749	48.6
		532 637	46.9
		588 822	49.0
		1 837 202	40.5
		2 074 945	40.5
Hole 8 mm	0.1	13 760	151.5
		14 887	150.4
		72 908	111.5
		112 023	112.3
		256 912	90.9
		359 662	90.2
		409 057	81.4
		465 304	80.8
Hole 3.5 mm	0.1	46 799	151.7
		55 969	150.6
		143 952	131.1
		150 272	132.1
		300 824	110.8
		364 965	110.8
		544 773	91.6
		1 232 012	91.0

Table A.7
Multiaxial experimental data of Fig. 5 obtained from Susmel and Taylor [62] for a load ratio of $R = -1$.

Multiaxial fatigue tests from Susmel and Taylor [62]					
Geometry	R	ϕ °	N_f	σ_a (MPa)	τ_a (MPa)
V-Notched 0.2 mm $\phi = 0$	−1	0	14 743	259.6	155.9
			30 837	216.3	129.9
			87 177	183.9	110.4
			460 400	146	87.7
			227 391	135.2	81.2
			924 890	135.2	81.2
V-Notched 0.2 mm $\phi = 90$	−1	90	67 416	183.9	110.4
			30 764	216.3	129.9
			210 914	146	87.7
			9202	259.6	155.9
			189 952	135.2	81.2
			1 646 841	129.8	77.9
V-Notched 0.2 mm *torsion*	−1	0	1 025 331	0	171.1
			31 705	0	264.8
			30 028	0	264.8
			306 633	0	171.1
			904 657	0	171.1
			344 380	0	203.7
			614 536	0	203.7
			70 232	0	244.5
			7700	0	297.4

(*continued on next page*)

Table A.7 (*continued*).

Multiaxial fatigue tests from Susmel and Taylor [62]					
Geometry	R	ϕ °	N_f	σ_a (MPa)	τ_a (MPa)
V-Notched 1.25 mm $\phi = 0$	−1	0	82 952	259.6	155.9
			437 907	200	115.5
			2 174 897	180	103.9
			46 254	275	158.8
			188 480	230	132.8
			1 400 006	190	109.7
V-Notched 1.25 mm $\phi = 90$	−1	90	314 817	260	150.1
			150 125	230	1f32.8
			59 622	270	155.9
			245 935	230	132.8
			79 328	250	144.3
			31 700	285	164.5
			36 976	285	164.5
V-Notched 4 mm $\phi = 0$	−1	0	282 833	290	167.4
			136 165	270	155.9
			38 446	330	190.5
			12 200	350	202.1
			57 847	280	161.7
			90 140	280	161.7
			11 543	370	213.6
			15 717	370	213.6
V-Notched 4 mm $\phi = 90$	−1	90	88 682	290	167.4
			7427	350	202.1
			51 504	270	155.9
			181 609	230	132.8
			6725	345	199.2
			266 899	245	141.5

Table A.8
Multiaxial experimental data of Fig. 5 obtained from Susmel and Taylor [62] for a load ratio of $R = 0$.

Multiaxial fatigue tests from Susmel and Taylor [62]					
Geometry	R	ϕ °	N_f	σ_a (MPa)	τ_a (MPa)
V-Notched 0.2 mm $\phi = 0$	0	0	11 899	162.2	168.7
			396 137	108.2	112.5
			626 504	97.3	101.2
			83 907	129.8	135
			6364	194.7	202.5
			6680	194.7	202.5
V-Notched 0.2 mm $\phi = 90$	0	90	62 951	129.8	135
			685 098	91.9	95.6
			45 580	146	151.9
			1 397 923	108.2	112.5
			203 792	119	123.7
			59 130	135.2	140.6
V-Notched 1.25 mm $\phi = 0$	0	0	844 615	150	150
			28 108	180	180
			370 618	160	160
			249 286	165	165
			34 298	190	190
			110 056	170	170
V-Notched 1.25 mm $\phi = 90$	0	90	112 944	170	170
			367 445	155	155
			49 200	180	180
			52 000	190	190
			67 873	200	200
			111 250	175	175
			304 439	160	160
			77 755	160	160
V-Notched 4 mm $\phi = 0$	0	0	60 384	250	144.3
			340 599	240	138.6
			316 599	230	132.8
			488 018	220	127
			422 875	245	141.5
			48 347	245	141.5
			721 275	200	115.5
			231 414	200	115.5

(*continued on next page*)

Table A.8 (*continued*).

Multiaxial fatigue tests from Susmel and Taylor [62]					
Geometry	R	ϕ °	N_f	σ_a (MPa)	τ_a (MPa)
V-Notched 4 mm $\phi = 90$	0	90	49 000	250	144.3
			106 129	245	141.5
			72 734	230	132.8
			60 399	235	135.7
			407 794	228	131.6
			165 543	224	129.3
			36 446	240	138.6
			31 641	240	138.6

References

[1] Morettini G, Braccesi C, Cianetti F, Razavi N, Solberg K, Capponi L. Collection of experimental data for multiaxial fatigue criteria verification. Fatigue Fract Eng Mater Struct 2020;43(1):162–74. http://dx.doi.org/10.1111/ffe.13101.

[2] European Committee for Standardization (CEN). Eurocode 3: Design of steel structures — Part 1-9: Fatigue, vol. 50. 2005, p. 77.

[3] Hobbacher AF. The new IIW recommendations for fatigue assessment of welded joints and components - a comprehensive code recently updated. Int J Fatigue 2009;31(1):50–8. http://dx.doi.org/10.1016/j.ijfatigue.2008.04.002.

[4] Fricke W, Gao L, Paetzold H. Fatigue assessment of local stresses at fillet welds around plate corners. Int J Fatigue 2017;101:169–76. http://dx.doi.org/10.1016/j.ijfatigue.2017.01.011.

[5] Karakaş, Zhang G, Sonsino CM. Critical distance approach for the fatigue strength assessment of magnesium welded joints in contrast to Neuber's effective stress method. Int J Fatigue 2018;112:21–35. http://dx.doi.org/10.1016/j.ijfatigue.2018.03.004.

[6] Radaj D, Sonsino CM, Fricke W. Fatigue assessment of welded joints by local approaches: second edition. 2006, p. 1–639. http://dx.doi.org/10.1533/9781845691882.

[7] Al Zamzami I, Susmel L. On the use of hot-spot stresses, effective notch stresses and the point method to estimate lifetime of inclined welds subjected to uniaxial fatigue loading. Int J Fatigue 2018;117:432–49. http://dx.doi.org/10.1016/j.ijfatigue.2018.08.032.

[8] Taylor D, Barrett N, Lucano G. Some new methods for predicting fatigue in welded joints. Int J Fatigue 2002;24(5):509–18. http://dx.doi.org/10.1016/S0142-1123(01)00174-8.

[9] Lazzarin P, Berto F. Some expressions for the strain energy in a finite volume surrounding the root of blunt V-notches. Int J Fract 2005;135(1–4):161–85. http://dx.doi.org/10.1007/s10704-005-3943-6.

[10] Berto F, Lazzarin P. The volume-based strain energy density approach applied to static and fatigue strength assessments of notched and welded structures. Procedia Eng 2009;1(1):155–8. http://dx.doi.org/10.1016/j.proeng.2009.06.036.

[11] Mroziński S. Energy-based method of fatigue damage cumulation. Int J Fatigue 2019;121:73–83. http://dx.doi.org/10.1016/j.ijfatigue.2018.12.008.

[12] Varvani-Farahani A, Haftchenari H, Panbechi M. An energy-based fatigue damage parameter for off-axis unidirectional FRP composites. Compos Struct 2007;79(3):381–9. http://dx.doi.org/10.1016/j.compstruct.2006.02.013.

[13] Braccesi C, Morettini G, Cianetti F, Palmieri M. Evaluation of fatigue damage with an energy criterion of simple implementation. Proc Struct Integr 2018;8:192–203. http://dx.doi.org/10.1016/j.prostr.2017.12.021.

[14] Fatemi A, Socie DF. A critical plane approach to multiaxial fatigue damage including out-of-phase loading. Fatigue Fract Eng Mater Struct 1988;11(3):149–65. http://dx.doi.org/10.1111/j.1460-2695.1988.tb01169.x.

[15] Findley WN. A theory for the effect of mean stress on fatigue of metals under combined torsion and axial load or bending. J Eng Indust 1959;81(4):301–5. http://dx.doi.org/10.1115/1.4008327.

[16] Kandil FA, Brown MW, J. MK. Biaxial low-cycle fatigue failure of 316 stainless steel at elevated temperatures. In: Mechanical behaviour and nuclear applications of stainless steel at elevated temperatures. London, UK: Maney Pub.; 1982.

[17] Huang J, Yang X, Shi D, Yu H, Dong C, Hu X. Systematic methodology for high temperature LCF life prediction of smooth and notched Ni-based superalloy with and without dwells. Comput Mater Sci 2014;89:65–74. http://dx.doi.org/10.1016/j.commatsci.2014.03.023.

[18] Cruces AS, Lopez-Crespo P, Moreno B, Antunes FV. Multiaxial fatigue life prediction on S355 structural and offshore steel using the SKS critical plane model. Metals 2018;8(12):1060. http://dx.doi.org/10.3390/met8121060.

[19] Olivier R, Köttgen V, Seeger T. Schweißverbindung I – schwingfestigkeitsnachweise für schweißverbindungen auf der grundlage örtlicher beanspruchungen. (welded joints I—Fatigue strength assessment method for welded joints based on local stresses). 1989.

[20] Radaj D. Review of fatigue strength assessment of nonwelded and welded structures based on local parameters. Int J Fatigue 1996;18(3):153–70. http://dx.doi.org/10.1016/0142-1123(95)00117-4.

[21] Niemi E, Fricke W, Maddox SJ. Fatigue analysis of welded components: Designer's guide to the structural hot-spot stress approach. Fatigue analysis of welded components: designer's guide to the structural hot-spot stress approach. Elsevier; 2006, p. 1–49.

[22] Lener G, Lang R, Ladinek M, Timmers R. A numerical method for determining the fatigue strength of welded joints with a significant improvement in accuracy. Proc Eng 2018;213:359–73. http://dx.doi.org/10.1016/j.proeng.2018.02.036.

[23] Taylor D. Geometrical effects in fatigue: a unifying theoretical model. Int J Fatigue 1999;21(5):413–20. http://dx.doi.org/10.1016/S0142-1123(99)00007-9.

[24] Susmel L, Taylor D. A novel formulation of the theory of critical distances to estimate lifetime of notched components in the medium-cycle fatigue regime. Fatigue Fract Eng Mater Struct 2007;30(7):567–81. http://dx.doi.org/10.1111/j.1460-2695.2007.01122.x.

[25] Sih GC, Madenci E. Fracture initiation under gross yielding: Strain energy density criterion. Eng Fract Mech 1983;18(3):667–77. http://dx.doi.org/10.1016/0013-7944(83)90058-9.

[26] Lazzarin P, Zambardi R. The equivalent strain energy density approach re-formulated and applied to sharp V-shaped notches under localized and generalized plasticity. Fatigue Fract Eng Mater Struct 2002;25(10):917–28. http://dx.doi.org/10.1046/j.1460-2695.2002.00543.x.

[27] Frendo F, Marulo G, Chiocca A, Bertini L. Fatigue life assessment of welded joints under sequences of bending and torsion loading blocks of different lengths. Fatigue Fract Eng Mater Struct 2020;43(6):1290–304. http://dx.doi.org/10.1111/ffe.13223.

[28] Palmieri M, Zucca G, Morettini G, Landi L, Cianetti F. Vibration fatigue of FDM 3D printed structures: The use of frequency domain approach. Materials 2022;15(3):854. http://dx.doi.org/10.3390/ma15030854.

[29] Chen F, Shang D-G, Li D-H, Wang L-W. Multiaxial thermo-mechanical fatigue life prediction based on notch local stress-strain estimation considering temperature change. Eng Fract Mech 2022;265:108384. http://dx.doi.org/10.1016/j.engfracmech.2022.108384.

[30] Chiocca A, Frendo F, Bertini L. Evaluation of heat sources for the simulation of the temperature distribution in gas metal arc welded joints. Metals 2019;9(11):1142. http://dx.doi.org/10.3390/met9111142.

[31] Chiocca A, Frendo F, Bertini L. Evaluation of residual stresses in a tube-to-plate welded joint. MATEC Web Conf 2019;300:19005. http://dx.doi.org/10.1051/matecconf/201930019005.

[32] Chiocca A, Frendo F, Bertini L. Evaluation of residual stresses in a pipe-to-plate welded joint by means of uncoupled thermal-structural simulation and experimental tests. Int J Mech Sci 2021;199:106401. http://dx.doi.org/10.1016/j.ijmecsci.2021.106401.

[33] Chiocca A, Frendo F, Aiello F, Bertini L. Influence of residual stresses on the fatigue life of welded joints. numerical simulation and experimental tests. Int J Fatigue 2022;162:106901. http://dx.doi.org/10.1016/j.ijfatigue.2022.106901.

[34] Meneghetti G, Campagnolo A, Visentin A, Avalle M, Benedetti M, Bighelli A, Castagnetti D, Chiocca A, Collini L, De Agostinis M, De Luca A, Dragoni E, Fini S, Fontanari V, Frendo F, Greco A, Marannano G, Moroni F, Pantano A, Pirondi A, Rebora A, Scattina A, Sepe R, Spaggiari A, Zuccarello B. Rapid evaluation of notch stress intensity factors using the peak stress method with 3D tetrahedral finite element models: Comparison of commercial codes. Fatigue Fract Eng Mater Struct 2022;45(4):1005–34. http://dx.doi.org/10.1111/ffe.13645.

[35] Wang WJ, Yim MS. A fatigue crack growth prediction model for cracked specimen under variable amplitude loading. Int J Fatigue 2023;168:107387. http://dx.doi.org/10.1016/j.ijfatigue.2022.107387.

[36] Susmel L. A simple and efficient numerical algorithm to determine the orientation of the critical plane in multiaxial fatigue problems. Int J Fatigue 2010;32(11):1875–83. http://dx.doi.org/10.1016/j.ijfatigue.2010.05.004.

[37] Marques JME, Benasciutti D, Carpinteri A, Spagnoli A. An algorithm for fast critical plane search in computer-aided engineering durability analysis under multiaxial random loadings: Application to the Carpinteri–Spagnoli–Vantadori spectral method. Fatigue Fract Eng Mater Struct 2020;43(9):1978–93. http://dx.doi.org/10.1111/ffe.13273.

[38] Wentingmann M, Noever-Castelos P, Balzani C. An adaptive algorithm to accelerate the critical plane identification for multiaxial fatigue criteria. In: Proceedings of the 6th European conference on computational mechanics: solids, structures and coupled problems, ECCM 2018 and 7th European conference on computational fluid dynamics, ECFD 2018. 2020, p. 3745–54.

[39] Sunde SL, Berto F, Haugen Br. Efficient implementation of critical plane for 3D stress histories using triangular elements. Int J Fatigue 2020;134:105448. http://dx.doi.org/10.1016/j.ijfatigue.2019.105448.
[40] Chow CL, Xu J. Application of the strain energy density criterion to ductile fracture. Theor Appl Fract Mech 1985;3(3):185–91. http://dx.doi.org/10.1016/0167-8442(85)90029-1.
[41] Macha E, Sonsino CM. Energy criteria of multiaxial fatigue failure. Fatigue Fract Eng Mater Struct 1999;22(12):1053–70. http://dx.doi.org/10.1046/j.1460-2695.1999.00220.x.
[42] Chen X, Xu S, Huang D. Critical plane-strain energy density criterion for multiaxial low-cycle fatigue life under non-proportional loading. Fatigue Fract Eng Mater Struct 1999;22(8):679–86. http://dx.doi.org/10.1046/j.1460-2695.1999.00199.x.
[43] Pedersen MM. Multiaxial fatigue assessment of welded joints using the notch stress approach. Int J Fatigue 2016;83:269–79. http://dx.doi.org/10.1016/j.ijfatigue.2015.10.021.
[44] de Freitas M, Reis L, Meggiolaro MA, de Castro JTP. Stress scale factor and critical plane models under multiaxial proportional loading histories. Eng Fract Mech 2017;174:104–16. http://dx.doi.org/10.1016/j.engfracmech.2016.12.016.
[45] El-sayed HM, Lotfy M, El-din Zohny HN, Riad HS. Prediction of fatigue crack initiation life in railheads using finite element analysis. Ain Shams Eng J 2018;9(4):2329–42. http://dx.doi.org/10.1016/j.asej.2017.06.003.
[46] Faruq NZ, Susmel L. Proportional/nonproportional constant/variable amplitude multiaxial notch fatigue: cyclic plasticity, non-zero mean stresses, and critical distance/plane. Fatigue Fract Eng Mater Struct 2019;42(9):1849–73. http://dx.doi.org/10.1111/ffe.13036.
[47] Hu Z, Berto F, Hong Y, Susmel L. Comparison of TCD and SED methods in fatigue lifetime assessment. Int J Fatigue 2019;123:105–34. http://dx.doi.org/10.1016/j.ijfatigue.2019.02.009.
[48] Bibbo ND, Baumgartner J, Arora V. Comparative study of critical plane fatigue criteria on multiaxial variable amplitude loaded welded test specimens. Int J Fatigue 2022;158:106670. http://dx.doi.org/10.1016/j.ijfatigue.2021.106670.
[49] Ran Y, Liu J, Wei Y. Probabilistic fatigue framework of notched specimens based on modified strain energy density model under multiaxial loadings. Eng Fract Mech 2022;266:108401. http://dx.doi.org/10.1016/j.engfracmech.2022.108401.
[50] Santus C, Taylor D, Benedetti M. Determination of the fatigue critical distance according to the line and the point methods with rounded V-notched specimen. Int J Fatigue 2018;106:208–18. http://dx.doi.org/10.1016/j.ijfatigue.2017.10.002.
[51] Santus C, Taylor D, Benedetti M. Experimental determination and sensitivity analysis of the fatigue critical distance obtained with rounded V-notched specimens. Int J Fatigue 2018;113:113–25. http://dx.doi.org/10.1016/j.ijfatigue.2018.03.037.
[52] Pedranz M, Fontanari V, Santus C, Lusuardi D, Berto F, Benedetti M. A strain energy density design approach for large cast iron components: From microstructural analysis to multiaxial fatigue response. Int J Fatigue 2023;175:107824. http://dx.doi.org/10.1016/j.ijfatigue.2023.107824.
[53] Karolczuk A, Skibicki D, Pejkowski Ł. Evaluation of the Fatemi-Socie damage parameter for the fatigue life calculation with application of the Chaboche plasticity model. Fatigue Fract Eng Mater Struct 2019;42(1):197–208. http://dx.doi.org/10.1111/ffe.12895.
[54] Santus C, Romanelli L, Grossi T, Bertini L, Le Bone L, Chiesi F, Tognarelli L. Elastic–plastic analysis of high load ratio fatigue tests on a shot-peened quenched and tempered steel, combining the chaboche model and the theory of critical distances. Int J Fatigue 2023;174:107713. http://dx.doi.org/10.1016/j.ijfatigue.2023.107713.
[55] Queiroz HS, Araújo JA, Silva CR, Ferreira JL. A coupled critical plane-area methodology to estimate fatigue life for an AISI 1045 steel with small artificial defects. Theor Appl Fract Mech 2022;121:103426. http://dx.doi.org/10.1016/j.tafmec.2022.103426.
[56] Araujo LC, de Oliveira D, Pereira MVS, Araújo JA. Adapted multiaxial fatigue models based on the critical plane approach to consider the presence of small defects in steel. In: Procedia structural integrity. 42, Elsevier; 2022, p. 163–71. http://dx.doi.org/10.1016/j.prostr.2022.12.020.
[57] Murakami Y, Endo M. Effects of defects, inclusions and inhomogeneities on fatigue strength. Int J Fatigue 1994;16(3):163–82. http://dx.doi.org/10.1016/0142-1123(94)90001-9.
[58] Liao D, Zhu SP, Qian G. Multiaxial fatigue analysis of notched components using combined critical plane and critical distance approach. Int J Mech Sci 2019;160:38–50. http://dx.doi.org/10.1016/j.ijmecsci.2019.06.027.
[59] Liu J, He Y, Wu K, Yi X, Wang J, Pan X. Probabilistic fatigue evaluation of notched specimens considering size effect under multiaxial loading. Eur J Mech A Solids 2023;102:105113. http://dx.doi.org/10.1016/j.euromechsol.2023.105113.
[60] Carpinteri A, Berto F, Campagnolo A, Fortese G, Ronchei C, Scorza D, Vantadori S. Fatigue assessment of notched specimens by means of a critical plane-based criterion and energy concepts. Theor Appl Fract Mech 2016;84:57–63. http://dx.doi.org/10.1016/j.tafmec.2016.03.003.
[61] Luo P, Yao W, Li P. A notch critical plane approach of multiaxial fatigue life prediction for metallic notched specimens. Fatigue Fract Eng Mater Struct 2019;42(4):854–70. http://dx.doi.org/10.1111/ffe.12956.
[62] Susmel L, Taylor D. The modified Wöhler curve method applied along with the theory of critical distances to estimate finite life of notched components subjected to complex multiaxial loading paths. Fatigue Fract Eng Mater Struct 2008;31(12):1047–64. http://dx.doi.org/10.1111/j.1460-2695.2008.01296.x.
[63] Chiocca A, Frendo F, Marulo G. An efficient algorithm for critical plane factors evaluation. Int J Mech Sci 2023;242:107974. http://dx.doi.org/10.1016/j.ijmecsci.2022.107974.
[64] Chiocca A, Sgamma M, Frendo F, Bucchi F. Rapid and accurate fatigue assessment by an efficient critical plane algorithm: application to a FSAE car rear upright. Proc Struct Integr 2023;47:749–56. http://dx.doi.org/10.1016/J.PROSTR.2023.07.044.
[65] Chiocca A, Sgamma M, Frendo F. Closed-form solution for the fatemi-socie extended critical plane parameter in case of linear elasticity and proportional loading. Fatigue Fract Eng Mater Struct 2023. http://dx.doi.org/10.1111/FFE.14153.
[66] Sgamma M, Chiocca A, Frendo F. Rapid and accurate semi-analytical method for the fatigue assessment with critical plane methods under non-proportional loading and material plasticity. Int J Fatigue 2024;182:108191. http://dx.doi.org/10.1016/J.IJFATIGUE.2024.108191, URL https://linkinghub.elsevier.com/retrieve/pii/S0142112324000495.
[67] Chiocca A, Sgamma M, Frendo F, Bucchi F, Marulo G. Fatigue assessment of a FSAE car rear upright by a closed form solution of the critical plane method. Frattura ed Integrità Strutturale 2024;18(67):153–62. http://dx.doi.org/10.3221/IGF-ESIS.67.11.
[68] Socie D. Multiaxial fatigue damage models. J Eng Mater Technol, Trans ASME 1987;109(4):293–8. http://dx.doi.org/10.1115/1.3225980.
[69] Chiocca A, Sgamma M, Frendo F. A closed-form solution for evaluating the Findley critical plane factor. Eur J Mech A Solids 2024;105:105274. http://dx.doi.org/10.1016/j.euromechsol.2024.105274.
[70] Mei J, Dong P. A new path-dependent fatigue damage model for non-proportional multi-axial loading. Int J Fatigue 2016;90:210–21. http://dx.doi.org/10.1016/j.ijfatigue.2016.05.010.